Digital holography as metrology tool at micro-nanoscale for soft matter

Zhe Wang[1,2], Lisa Miccio[1,3], Sara Coppola[1,3], Vittorio Bianco[1], Pasquale Memmolo[1],
Volodymyr Tkachenko[1], Vincenzo Ferraro[2], Ernesto Di Maio[2], Pier Luca Maffettone[2,3]
and Pietro Ferraro[1,3,*]

Abstract

The appearance of the first laser approximately 12 years after the invention of holography by Gabor (1948) revolutionized the field of optical metrology. In fact, the invention of holographic interferometry enabled the exploitation of interferometry on non-mirror surfaces and full-scale objects. The holography-based measurement methods has been implemented to several industrial systems or in support of R&D with the aim of improving new products in many fields (automotive, aerospace, electronics, etc.). To date, holography has been considered an important measurement tool for non-destructive inspection (NDI), strain-stress measurement, and vibration analysis at various engineering sites. Recently, the new paradigm of Industry4.0 has seen the introduction of new technologies and methods of processing materials as well as the development of manufacturing approaches for the realization of innovative products. For example, direct printing, additive, and bottom-up manufacturing processes are expected to involve new ways of making products in future, and most innovative fabrication processes will be based on the manipulation of soft matter (e.g., starting from the liquid phase) that will be shaped at the nanoscale. The inherent characteristics of digital holography (DH) make it a powerful and accurate tool for the visualization and testing of final products, as well as for in situ and real-time monitoring and quantitative characterization of the processes involved during the fabrication cycle. This review aims to report on the most useful applications of soft matter, where the capabilities offered by DH, such as three-dimensional (3D) imaging, extended focus, 3D tracking, full-field analysis, high sensitivity, and a wide range of measurements from nanometers to centimeters, permit completely non-invasive characterizations on a full-scale. Several holographic experimental results of typical samples are reported and discussed where DH plays a primary role as a tool gauge for soft matter.

Keywords: Digital holography, Soft matter, Microscopy, Thin film, Polymers, Liquids, Characterization, Interferometry, Inkjet printing

Correspondence: Pietro Ferraro (p.ferraro@isasi.cnr.it)
[1]CNR-ISASI, Institute of Applied Sciences and Intelligent Systems "E. Caianiello", Via Campi Flegrei 34, 80078 Pozzuoli, Napoli, Italy
[2]Dipartimento di Ingegneria Chimica dei Materiali e della Produzione Industriale, Università degli Studi di Napoli "Federico II", Piazzale Tecchio 80, 80125 Napoli, Italy
Full list of author information is available at the end of the article.
These authors contributed equally: Zhe Wang, Lisa Miccio, Sara Coppola

Introduction

The most important advantage arising from the invention of holography was realized with the development of lasers. The applications of holography has been exploited in many industrial fields as a very sensitive measurement tool, such as aerospace, automotive, energy and cultural heritage,

owing to the discovery of holographic interferometry by Powell and Stetson[1,2]. In fact, by employing different holographic modalities, such as holographic interferometry, time-average holography, or the so-called TV and/or digital speckle holography, it was possible to develop accurate optical measuring strategies for non-destructive testing systems and experimental mechanics[3,4]. The above holography-based measurement systems were applied successfully to guarantee the quality of industrial products (e.g., turbine blades, tires, composite materials, photovoltaic solar panels, automobile components, and electronic circuits). Later, with the microelectronic revolution in the 80s and 90s as well as the surge of capabilities of micro-nanofabrication techniques, holography-based methods were successfully applied by scaling their probing-gauge down to microsystems (i.e., MEMS, MOEMS, and NEMS)[5–10]. In the past 20 years, the introduction of powerful PCs and high-performance solid-state light sensors has resulted in the achievement of further developments of holographic technology in digital-modality toward biological, biomedical, and industrial applications, which has led to the widespread use of such systems[11–16].

Recent progress in bottom-up self-assembly fabrication approaches and direct printing for production processes, especially at the micro and nanoscales, has motivated the development of holographic optical tools for achieving accurate and full-field characterization of systems based on soft matter materials, such as liquids and polymers. These are expected to be the basis of the next revolution in fields of biotechnology and flexible electronics systems, among others. Indeed, the most common imaging modality for such microfabrication techniques is direct optical imaging, which is a video-based method. It enables the monitoring of the dynamic evolution of the processes and measuring features related to the geometrical dimensions of the microstructure[17,18]. High-speed and high-resolution cameras were used for the detection of small particles during inkjet printing. Although such imaging systems can be complex, significant information is completely lost as in the case of the detection and measurement of out-of-focus structures and particles. Furthermore, not all of the information related to the phase shift introduced by the samples can be evaluated. Many microstructures are transparent or semi-transparent, and it is critical to measure the phase delay introduced in the light path, as in the case of the evaluation of the optical quality of optical components, such as microlenses and thin-film thickness mapping at high spatial resolution. For these reasons, the inspection of soft matter and related fabrication processes takes advantage of the noteworthy capabilities of DH as a metrology tool. As summarized below, the main attractive features of DH enable the achievement of the necessary capability and flexibility in the measurements:

1) The possibility of numerically managing the complex wavefront scattered or transmitted by the sample under investigation allows the extraction of all of the information (intensity and phase) through a full-digital modality.

2) Flexibility in achieving object imaging well-in-focus (or to obtain good focus of any portion of it) that enables correct DH microscopic measurements to be obtained, even though the object could have a three-dimensional (3D) shape behind the depth of focus of the optical imaging system.

3) Potential to retrieve phase-contrast maps that enable quantitative measurements of the sample in full-field mode and 3D.

4) The possibility to manage and remove aberrations in the optical system using simple and flexible methods, thus simplifying the optical apparatus and measurement operations.

Owing to the above unique features of DH, this paper reviews what are considered the most significant examples to demonstrate the capability of DH to measure soft matter structures and the related fabrication techniques. In particular, we focused on different types of challenging cases.

• thin liquid films and membranes;

• ink-jet printing process for directly printed structures;

• analysis and quantitative measurements of bottom-up self-assembling processes of polymer and/or liquids;

• microfluidic rheology and study of solid-liquid interfaces.

The four different above-mentioned typical cases enable us to demonstrate the aptitude of DH systems in combining metrology and 3D imaging capabilities and by furnishing quantitative measurements in challenging circumstances. We show that 3D dynamic monitoring in real-time or in situ using DH enables quantitative measurements and accurate characterization.

It should be noted that biological matter, both cell populations and tissues, benefits from the above-mentioned characteristics, so DH in recent years has been extensively developed, enabling its incorporation in life sciences[19–26]. However, we focus on and limit the present review to fabrication topics, thus supplying a complete overview of DH in this area without including cells of biological matter that have different peculiarities.

This review is organized into three sections. The first focuses on the measurement of the thin-film thickness over a wide field of view (FoV). Various experimental configurations are described, and their applicability to

different materials is provided. For such applications, the thickness measurement ranges from ~50 nm to ~30 μm, with a resolution at the nanometer scale on a large FoV of a circular area with a radius of ~20 mm. The second section is centered on a specific microfabrication technique based on the exploitation of the pyroelectric effect of ferroelectric crystals, where liquids and polymers can be manipulated by electric fields. This enables us to provide many examples where DH has proven to be a suitable metrological tool not only for transparent solid microstructures but also for the full characterization of dynamic processes such as the self-assembly of liquids for the realization of microstructures. The main results show that high-resolution two-dimensional (2D) and 3D measurements can be achieved by exploiting the quantitative phase content encoded in the digital holograms. The third section presents DH to investigate the rheological properties, monitor stress, and track particles embedded in solution or liquid film. All three sections contain a detailed description of the related state-of-the-art. Different setups and target materials, in addition to diverse observables, are described and discussed in this manuscript.

Digital holography for studying thickness evolution of thin liquid films

From soap bubbles for children to semiconductors for electronics, thin films have accompanied humankind through countless centuries, and are an important category of soft matter. Over the past century, with the improvement in industrial production technologies, a large number of products related to thin-film materials have been produced, especially in the field of daily chemistry. With the informatization and intelligence of human society, wearable and in-body devices are becoming the general direction of future technology applications. Because of its special physical and chemical properties, film material has become the best carrier to support future devices, and a detailed measurement of its characteristics is highly desirable.
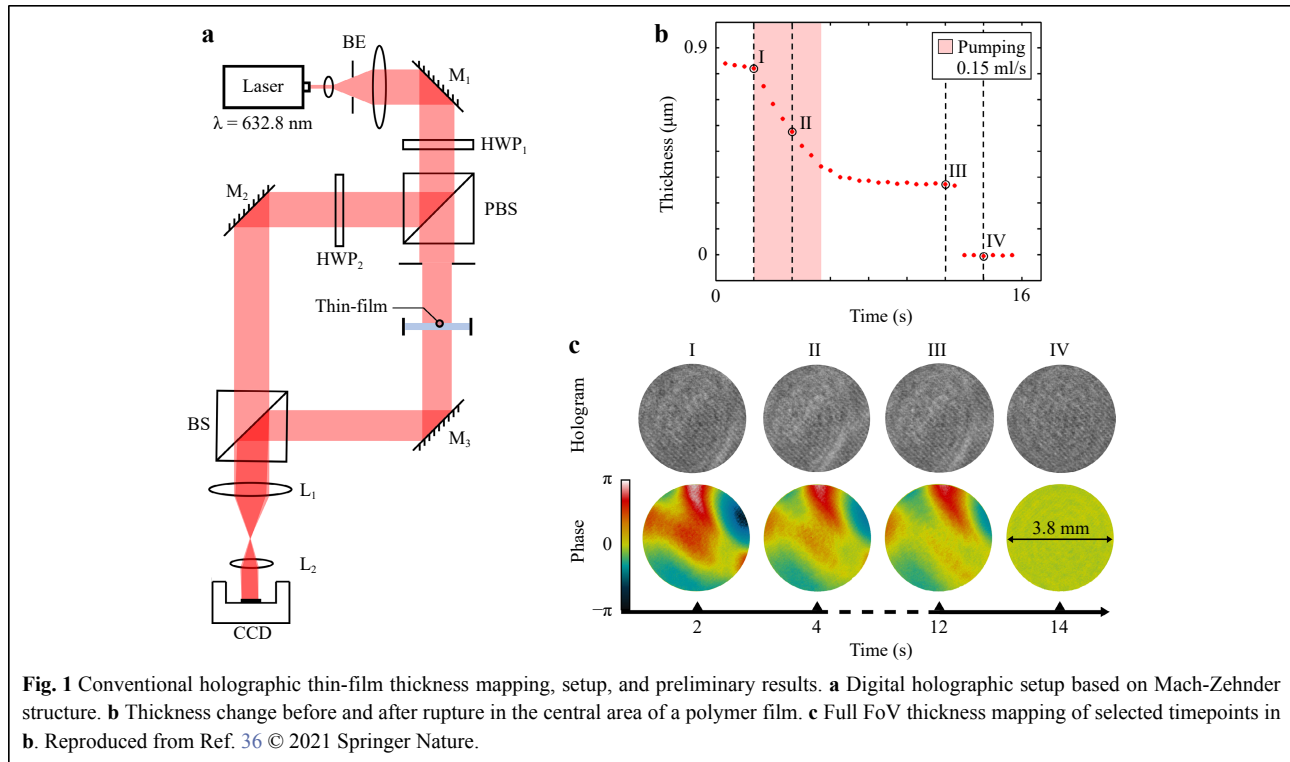
The mapping of the thin-film thickness is an open and long-term challenge[27]. One of the well-known methods for mapping film thickness is the interferometric approach[28], which uses the optical path difference between the beam's reflection of the upper and lower surfaces of the film to create an interferometric pattern from which the thickness information of the thin film can be determined[29,30]. The interferometry method has been used for a long time. However, conventional interferometric measurements have some shortcomings, such as a small measurement FoV, limited measuring range, and non-real-time measurement.

To overcome these drawbacks, a series of interferometric techniques has been proposed in recent decades, namely colorimetric interferometry[31,32], multiwavelength interferometry[33], phase-shift interferometry[34], and scanning interferometry[35], etc. However, for the dynamic thickness measurement of a thin liquid film under a large FoV, interferometric methods hardly meet all recording requirements, especially for films with high viscosity coefficients. In 2019, for the first time, Ferraro et al. implemented DH to map the thin-film thickness during the evolution of liquid bubbles[36]. In 2021, Wong et al. applied DH to measure beer bubble morphology[37]. The height of the beer bubbles and water surface can be revealed simultaneously by the back-propagation process of DH. In fact, most film materials are good samples for holographic measurements because of their transparent or semi-transparent properties[38]. However, the existence of micron-level deformation in the film evolution generates scattering and/or refraction for object beam, which significantly affects holographic recording. This problem was solved by introducing a telescope structure before the camera, which could collect the beams and adjust the magnification. As a result, real-time holographic measurements of thin-film thickness were successfully realized. Many thin-film measurement experiments have been conducted using holography in different scenarios. In the following subsections, we systematically introduce the applications of DH in thin-film measurements and explore the feasibility of the technique in the measurement of soft matter.

Basic principle and experimental setup of digital holographic film imaging

The primary problem faced by DH in thin-film measurement is the limited thickness measurement range in a single shot[39]. There is a specific measurement range for the holographic recording of laser sources in the visible spectral range. Moreover, owing to the influence of surface tension, the thickness distribution of thin-film materials is usually continuous, enabling numerical holographic phase unwrapping. Considering the real-time requirements of film thickness measurement, the off-axis DH system could be a good candidate for testing[14,40]. In preliminary optical geometry, an off-axis Mach-Zehnder recording system was used to measure the dynamic film thickness evolution process[36,41]. A telescope structure was set before the camera to adjust the FoV and suppress the influence of film scattering (the setup and experimental results are shown in Fig. 1.

Because thin films represent imaging objects with rich and varied high-frequency information, it is difficult for a

Fig. 1 Conventional holographic thin-film thickness mapping, setup, and preliminary results. **a** Digital holographic setup based on Mach-Zehnder structure. **b** Thickness change before and after rupture in the central area of a polymer film. **c** Full FoV thickness mapping of selected timepoints in **b**. Reproduced from Ref. 36 © 2021 Springer Nature.

lens-less system to collect all information during the recording process. Therefore, a telescope structure (composed of two lenses with different focal lengths) represents a strategy for collecting object information. As shown in Fig. 1a, lenses L_1 and L_2 (focal length of L_1 is longer than that of L_2) were set to construct a telescope lens group for zooming out. The light-collecting ability of the 4-Focus lens group allowed the collection of scattered object beams. In other words, this setup allowed the enlargement of the FoV and the simultaneous recording of high-frequency information. In the initial testing, a film close to rupture was selected as the sample. The thickness change in the central area of the film was measured[41], as shown in Fig. 1b. It can be seen that for thin-film materials with a known refractive index (RI), DH is a good tool for measuring the thickness of the film, and it does not require other reference images. Generally, in interferometry, it is necessary to clearly observe the appearance of a common black film[42] to obtain absolute thickness measurements. However, for holographic measurements, when the thickness of the film is less than twice the recording wavelength, the following phase-thickness conversion formula can be used directly to extract the thickness information from the phase map:

$$h = \frac{\varphi\lambda}{2\pi n} \tag{1}$$

where h is the thickness, φ is the phase, λ is the recording

wavelength, and n is the RI of the film. For the range of thickness measurement in a holographic recording system with a specific laser wavelength, the lower limit depends on the wavelength, whereas the upper limit can be continuously increased owing to the holographic phase unwrapping algorithm. Here, PUMA[43] phase unwrapping is a good candidate for extracting film thickness information because of its good phase-unwrapping capabilities for a continuously changing phase. However, in the case of films where the maximum thickness reaches a few micrometric levels or even higher, conventional holographic reconstruction will not be able to implement absolute thickness measurements owing to the limitation of the wrapping phase. To solve this problem, a full life cycle measurement method was proposed[36]. To do this, the entire thickness evolution process of the film, from the initial formation to the final rupture, needs to be recorded. Once the film is close to rupture, the starting area of the rupture tends to be a common black film, indicating that it has the lowest phase value in the full FoV. Taking advantage of this feature, a time variable can be added to the phase-unwrapping process to deal with the phase jump in all recorded frames, as shown in Fig. 2.

As a film thickness extraction scheme, the full life cycle recording method has certain limitations; in fact, the measured film must have a clear natural rupture process. For most free-standing thin liquid films, the natural rupture
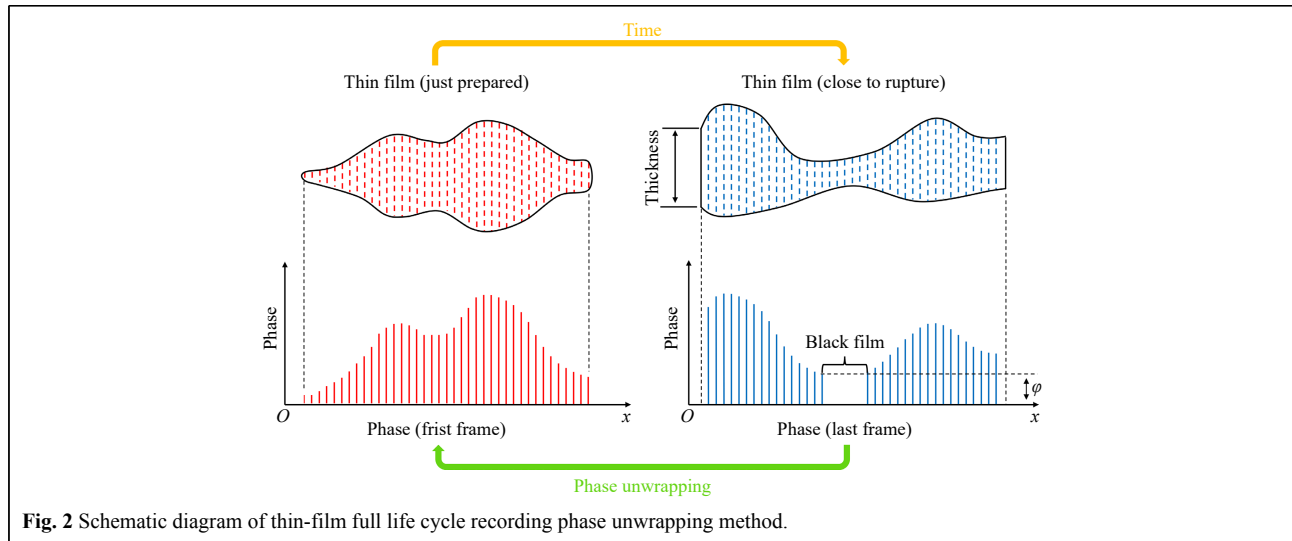
Fig. 2 Schematic diagram of thin-film full life cycle recording phase unwrapping method.

process will occur owing to gravitational drainage[44], which enables us to use the proposed strategy for extracting film thickness information. Therefore, compared to other existing optical measurement methods, DH offers high precision, a large measurement range, and real-time characteristics, representing a good tool for thin liquid film thickness mapping, as discussed in detail in the following sections.
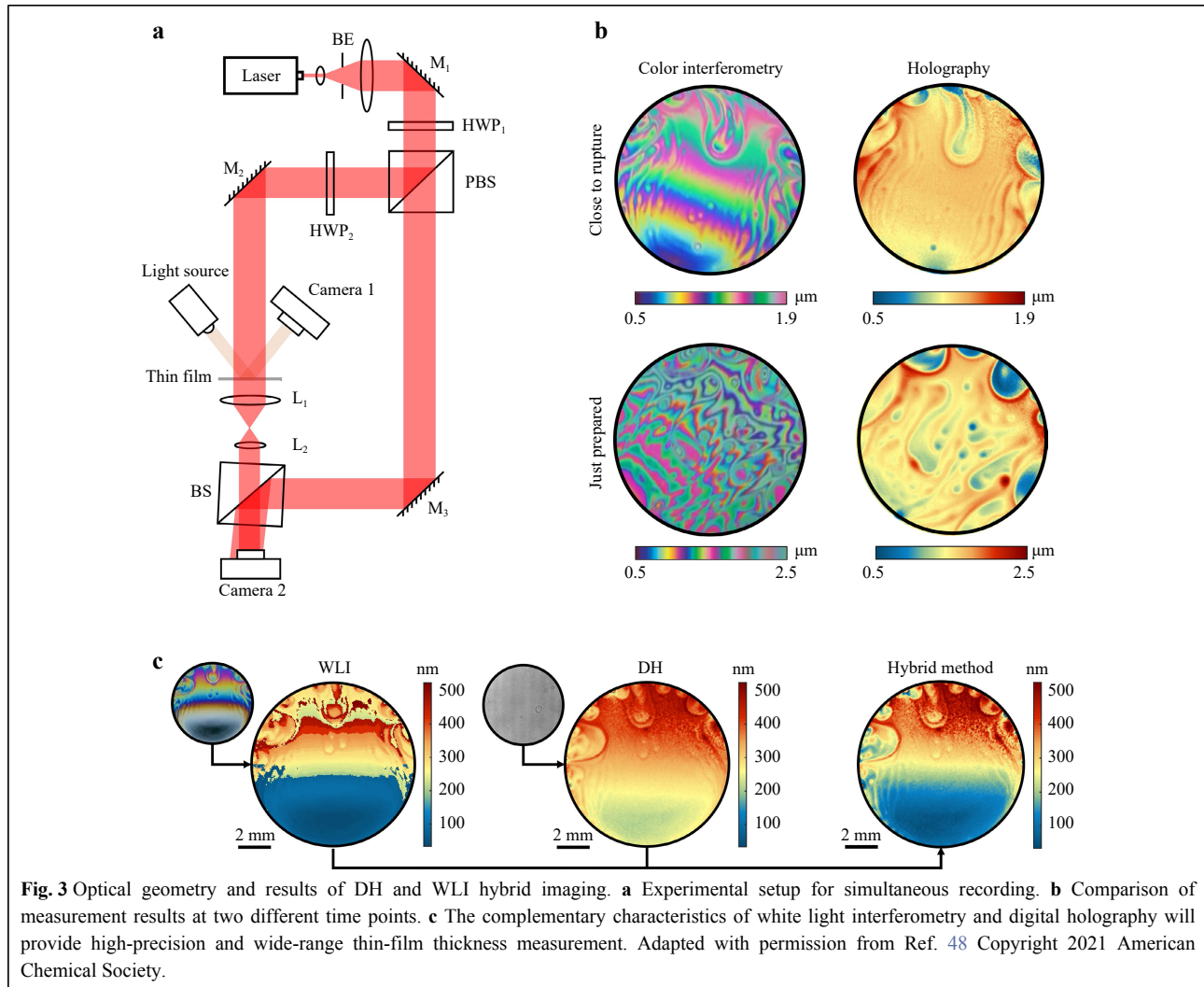
Joint-measurement between white light interferometry and digital holography

DH is based on the numerical diffraction reconstruction of digitally recorded interference fringes to obtain the spatial information of the recorded object[45,46], whereas white-light interferometry (WLI) uses the direct identification of the number and color of interference fringes to obtain thickness information[28,29]. These two methods have certain limitations in real-time thin-film thickness mapping, but for some specific materials, both can be used, for example, surfactant film. Thus, the complementary characteristics of WLI and DH enable comparison and fusion. To implement simultaneous recording for one liquid film using the two methods, joint imaging was designed by combining the conventional off-axis DH geometry and WLI geometry. To ensure that the WLI recording did not affect the intensity contrast of the hologram, oblique illumination was implemented[47]. Owing to the combination of WLI and DH, it is possible to achieve high-precision real-time thickness measurements while expanding the imaging FoV and range[48]. The experimental setup, which combines the two interferometric geometries, is shown in Fig. 3a.

In the experiment reported in Fig. 3b, a surfactant film was selected as the experimental sample, and its RI was

determined in a previous study[49]. Meanwhile, for the WLI measurement, the thickness-color correspondence of the surfactant film is known[50]. The surfactant film was formed in a fixed metal ring and simultaneously illuminated by white light and a red laser beam. It can be seen from the experimental results in Fig. 3b that when the film was close to rupture, both DH and WLI could map the thickness of the full FoV. Based on the comparison, it can also be found that the measurement results of DH and WLI maintain good consistency in the range below 1 µm. Moreover, for a thickness greater than 1 µm, WLI hardly provides the right thickness value, while DH still works. For the results at the early stage after film formation, the WLI interferogram showed complicated patterns; thus, it was difficult to interpret and retrieve the effective thickness. The colored interference fringes in such a range of film thicknesses were spatially and periodically modulated by the complex film structure, which led to an impossible reading. On the other hand, the thickness distribution information can be clearly identified in the results of DH. This is the greatest advantage of holographic measurement: for films with complex structures, holographic measurement can still provide an accurate thickness distribution. In conclusion, for surfactant films with a maximum thickness of less than 1 µm and a smooth surface structure, both DH and WLI can be used. However, for films with a higher thickness or complex surface structure, DH would be a better choice. Therefore, the reliability of the DH measurements can be verified through WLI experiments.

However, in the case of film with thickness less than half the wavelength, transmission holography has difficulties in providing accurate thickness measurements. Therefore, one strategy that has been effectively adopted is to use the complementary characteristics of WLI and DH

Fig. 3 Optical geometry and results of DH and WLI hybrid imaging. **a** Experimental setup for simultaneous recording. **b** Comparison of measurement results at two different time points. **c** The complementary characteristics of white light interferometry and digital holography will provide high-precision and wide-range thin-film thickness measurement. Adapted with permission from Ref. 48 Copyright 2021 American Chemical Society.

for a new hybrid measurement modality[48]. Thus, phase correction was achieved by comparing the two different measurement results. From the results in Fig. 3c, the deviation in the low-thickness area was significantly improved; essentially, the hybrid recording and reconstruction completed the phase calibration of the film and achieved an accurate thickness distribution. As a tool for improving microscopic resolution, holographic imaging can be easily integrated with other technologies, creating a wider range of possibilities.

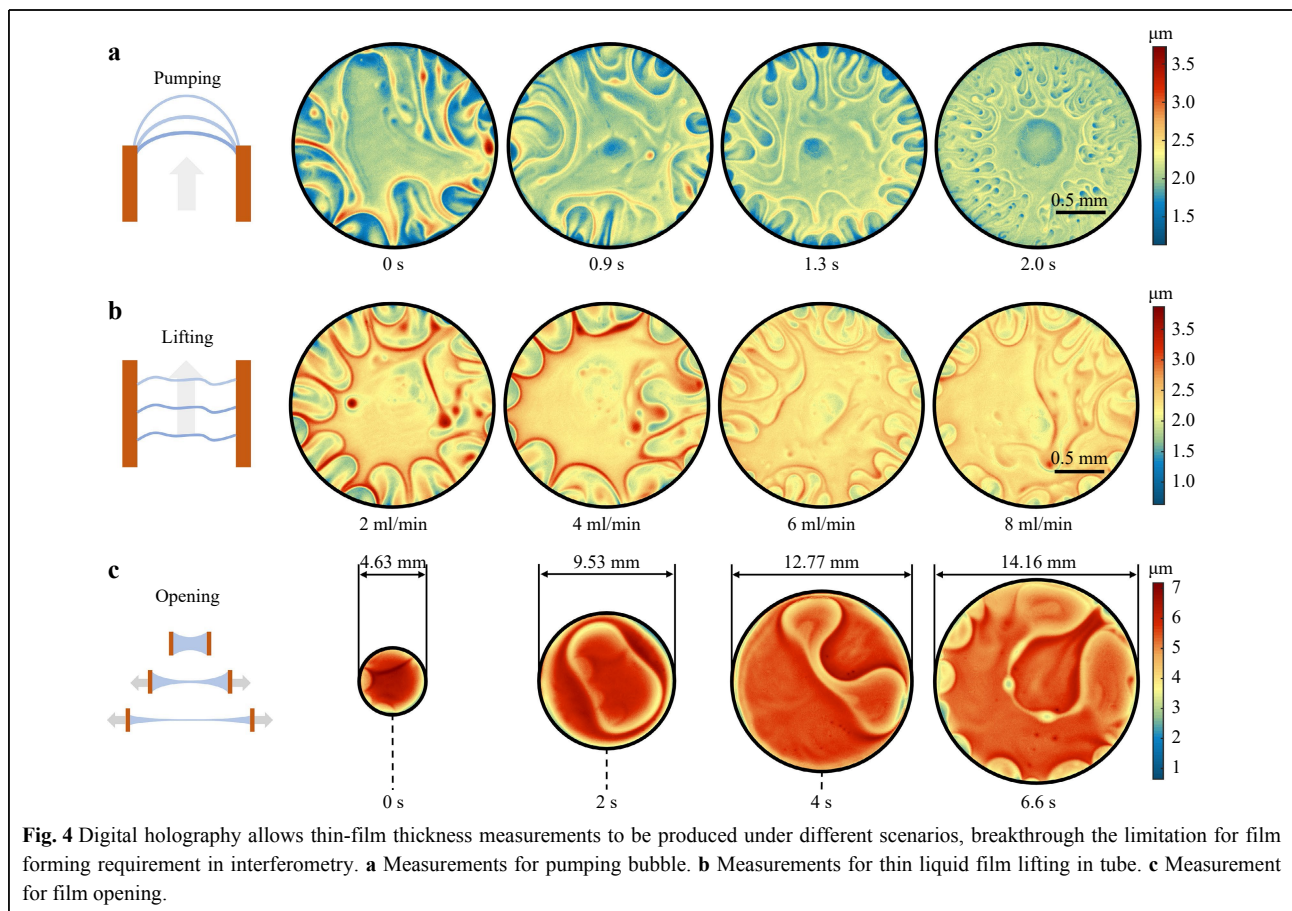**Suitability of digital holography in different thin-film experimental arrangements**

In the above two sections, conventional imaging setups and methods of DH in thin-film imaging were discussed for the measurement of the thickness level. Furthermore, the difference between the results of WLI and DH for the same film was compared, proving that DH is a reliable

measurement method for thin films. In conventional interferometric experiments, the measurement methods and systems are limited because of the need to keep the sample as smooth as possible. In addition, because the distance between the camera and the sample has certain requirements for creating interference fringes, it is difficult to measure the thickness distribution when the film is moving. However, these limitations can be overcome for DH recording. The DH geometry has good flexibility in structural settings; therefore, it can deal with different experimental scenarios[51]. Meanwhile, thanks to the numerical diffraction propagation process, DH can present real-time thickness mapping for the film in motion. Fig. 4 shows the time-lapse recording results obtained by DH in different film motion modes, including pumping bubble, thin film lifting, and thin film opening. Thickness mapping for these processes appeared to be difficult during interferometric recording, but could be completed in DH

recording.

In an experiment on pumping liquid bubbles, a flat thin film was prepared at one end of a customized tube, and air was pumped into the tube to promote bubble growth. Finally, a semicircular bubble was formed[36]. The transmissive DH can effectively record the thickness of the bubble during the growth process, and then the thickness information extraction can be completed through numerical refocusing and phase distortion calibration. Fig. 4a shows the measurement results of related experiments. In this experiment, a polyacrylamide (PA) solution was used to create a thin liquid film. For this kind of film, the reconstruction of thickness mapping could be provided using the full life cycle recording method. In addition, owing to the phase distortion calibration, the hemispherical film thickness distribution can be projected as a horizontal mode, which is convenient for researchers to analyze the drainage process. For the lifting thin-film experiment, the film was prepared in the middle of a customized tube and then lifted by pumping air into the tube from the bottom. Because of the centimeter-level movement of the film inside the tube, conventional interferometric methods were unable to provide the thickness distribution during the

movement; however, DH could solve this problem. Fig. 4b shows the results of related experiments. The drainage phenomenon in the process of film uplift is related to the velocity of movement, which introduces the potential for controllable drainage. This will help to better study the physical model of the drainage process. The results showed the distribution of the film structure at different moving speeds, and the difference in drainage patterns was revealed. For the film-opening experiments, an optical iris was conceived and manufactured to open the film[52]. Then, an adjusted telescope structure was used to reach a large FoV (~40 mm diameter), which ensured the recording of the entire film area during the film-opening process. This is also a significant advantage of holographic measurement; the FoV can be changed by adjusting the lens group, thereby realizing continuous holographic recording with a large FoV. The opening process of the film included a potential change in the overall film thickness from high to low. This experimental system ensured that the total amount of solution used to prepare the film remained constant, thereby facilitating the analysis of the hydrodynamic process. Fig. 4c shows the results of related experiments.

Fig. 4 Digital holography allows thin-film thickness measurements to be produced under different scenarios, breakthrough the limitation for film forming requirement in interferometry. **a** Measurements for pumping bubble. **b** Measurements for thin liquid film lifting in tube. **c** Measurement for film opening.

In the above three experimental scenarios, holographic measurements showed good thickness measurement capabilities. For most experimental environments, the holographic setup can be easily changed to meet the requirements of recording, enabling its application in the field of fluid mechanics testing.

Digital holography performances on different materials

The term "thin film" is ubiquitous in our daily lives, and includes a broad range of materials, from solid to liquid films. In general, under the conditions of interferometric measurements, different configurations are used to complete experiments on different matters. For example, tilted WLI is mainly used for liquid films[20], whereas a vertical interferometric system is required for solid films, such as semiconductors of the indium tin oxide (ITO) layer[53]. In this section, we show the measurement results for films made of different matter to demonstrate the good adaptability of the DH technology in film measurements.

The main problem with conventional interferometric measurements is that it is difficult to realize real-time imaging with a large FoV. In recent years, some methods have been proposed to solve this problem[54], but certain restrictions on the RI and film thickness have been added. However, DH recordings are not affected by these limitations. Fig. 5 shows liquid films prepared using three different solutions: surfactants[48], polyacrylamide (PA)[36], and polydimethylsiloxane (PDMS)[52].

Although we can observe differences in the thickness and morphology of the different films, as shown in Fig. 5, the DH system successfully recorded thickness information. For transmissive holographic recording, light transmittance and polarization of the recording object must be considered. For thin-film materials, most liquid films have good light transmittance, and their polarization effects are so small that they can be ignored. Therefore, holographic measurements can be used for most transparent thin liquid films. Compared with liquid films, solid films are more difficult to image; a main reason is the molecular spacing of the solid films is closer than that of the liquid film, which means that the RI of solid films is generally greater than that of liquid films. Currently, the measurement technology for solid nonuniform thin films remains an unresolved challenge. Many factors limit conventional measurement methods[55], although some initial results have been obtained[30]. From the above experiments, holography has shown excellent measurement capabilities for different materials, is not limited to physical properties, and can successfully provide measurements for most of thin-film materials. This is a very interesting feature that challenges the stringent requirements of interferometry for samples.
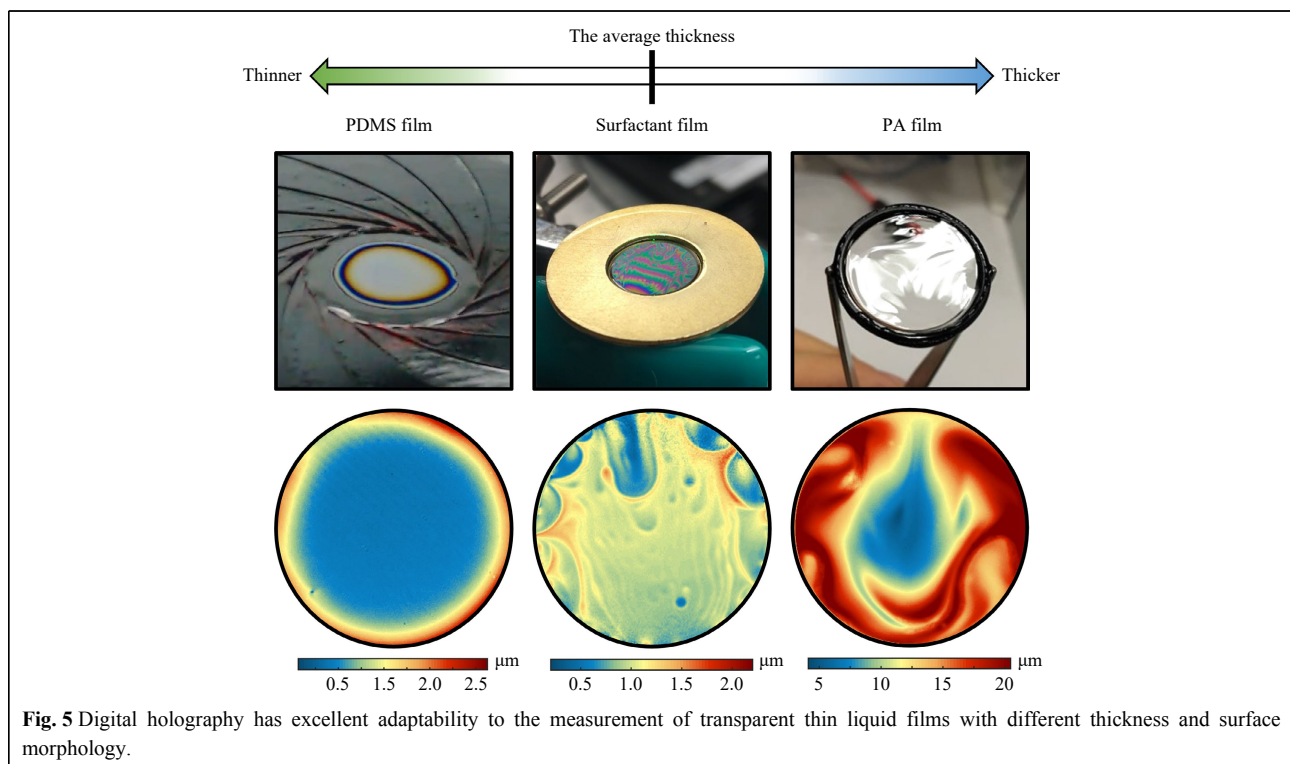

Fig. 5 Digital holography has excellent adaptability to the measurement of transparent thin liquid films with different thickness and surface morphology.
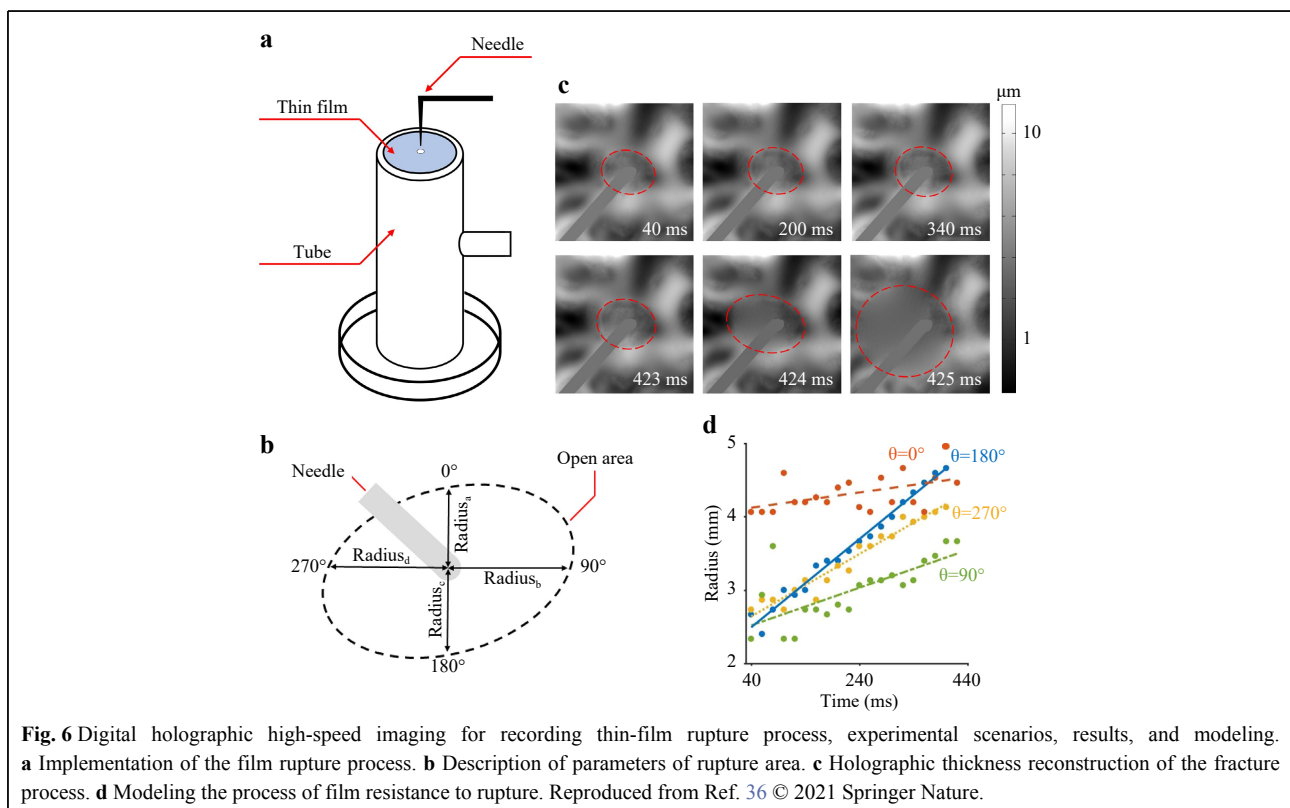
High-speed holographic recording for thin-film rupture

In the previous sections, the film imaging process at a standard recording speed was discussed. However, for holographic recording systems, owing to the excellent real-time imaging capabilities in off-axis geometry, it is possible to use a high-speed CMOS camera to dynamically follow the thickness evolution. Among these, the rupture process of films is a widely studied issue. For a long time, there has been no reliable measurement technology to capture the edge morphology during film rupture, and DH technology can therefore fill this gap.

The film rupture process can be easily imaged using a conventional off-axis holographic setup with a high-speed camera (980 fps). The related process was modelled to describe the rupture mechanism[33]. From the time–space model in Fig. 6c, it can be observed that after using the needle to break the film, it resists the rupture process. These results were revealed using holographic technology for the first time. We believe that relevant experimental data will provide important data support for researchers in fluid mechanics. In fact, many microfluidic phenomena occur very quickly and can be analyzed with the help of DH.

Digital holography for inkjet printing, additive manufacturing and advanced fabrication techniques

The electrohydrodynamic (EHD) manipulation of liquids is becoming an increasingly popular topic owing to its application in physical, chemical, biological, and engineering research areas, such as microdetectors, the micro-dispensing of small sub-nanoliter volumes of fluids for sensors, flat panel displays, and biochips[56]. EHD inkjet printing relies on the generation of droplets at or near a nozzle aperture, followed by noncontact deposition on a substrate with high spatial control. Recently, an interesting approach based on the use of a virtual nozzle on the pyroelectric forces has been introduced and applied for the manipulation and dispensing of liquid inks ranging from low to high viscosity. The pyroelectric effect involves the delivery of materials to surfaces at micrometer and nanometer length scales without nozzles or electrodes. The local heating induced on pyroelectric substrates, such as lithium niobate (LN), generates an electric field through the well-known pyroelectric effect[57–60]. Beyond a threshold electric potential, this field pulls ink from the free liquid surface of the reservoir to form a conical jet similar to the Taylor cone. Controlling the translation of an additional substrate inserted between the LN and the opposing

Fig. 6 Digital holographic high-speed imaging for recording thin-film rupture process, experimental scenarios, results, and modeling. **a** Implementation of the film rupture process. **b** Description of parameters of rupture area. **c** Holographic thickness reconstruction of the fracture process. **d** Modeling the process of film resistance to rupture. Reproduced from Ref. 36 © 2021 Springer Nature.

substrate with a liquid reservoir allows additive patterning of the ink materials. The use of pyroelectric effects has provided new capabilities that have been demonstrated in different application contexts, from high-resolution printing and patterning to the fabrication of customized polymeric microstructures[61–64]. Pyro-inkjet and EHD-printing in general have an interesting physical mechanism leading to diverse jetting behaviors according to the operating conditions and physicochemical properties of the liquid, such as surface tension, viscosity, electric conductivity, and relative permittivity[65]. Considering that EHD may be applied to different fields according to various ejection conditions, the visualization and understanding of the printing mode would result in better control of the entire fabrication process. Commonly, most of these modes are observed using only one camera, which is only appropriate for stable symmetric modes such as dripping, microdripping, and cone-jet modes, and not for other unstable asymmetric modes. In the case of unstable trajectories, such as the multispindle mode, oscillating-jet mode, precession, and multijet mode[66,67], 3D visualization is necessary to follow the trajectory and exact locations of the ejected droplets. To address this limitation, a 3D tomographic technique was proposed to study the unstable ejection phenomena of droplets[68]. In addition, the shadowgraphic tomography technique was implemented to reconstruct jetting three-dimensionally[69–71]. Recently, a numerical method for reconstructing the 3D phenomena was proposed to solve the problem of the invisible area by multiplicative line-of-sight (MLOS) and ellipse estimation; however, the experimental procedures are still long-lasting and complicated[69]. Even if good results have been obtained by non-intrusive measurement tomography, the setup required for the measurement is still very expensive, requiring more than two cameras, optical components, and dedicated software. In fact, to reconstruct acceptable results from limited projection data, different tomographic algebraic algorithms have been combined, which require time and computational resources[70,71]. Recently, quantitative phase microscopy (QPM) has been demonstrated to be a valid tool for the evaluation of liquid and polymer droplet characteristics. In Ref.[72], the authors reported on real-time quantitative phase imaging for measuring the evaporation dynamics of sessile microdroplets. The surface wetting properties were retrieved by 3D topographic profiles with nanometer accuracy. QPM has also been used to demonstrate the ability to observe nanosized, semi-transparent, structured coatings involving two materials by combining high-resolution maps of optical path differences and electrical impedance variations[73]. In this framework, DH microscopy

was used to investigate the wetting properties of ink dots obtained by direct writing on a glass plate[74]. Even though the proposed method could track the temporal evolution of the height, volume, and contact angle of the printed ink dots of approximately 200 mm from gelation to solidification, no report exists that explains the quantitative visualization of 3D viscous polymers, which usually have a high aspect ratio and a trajectory that could span long distances in the FoV[75]. The quantification of polymeric objects, which rely heavily on manual operations, is labor-intensive and lacks accuracy. In the literature, we found some experiments involving simple cases such as needle and fiber entities, in which the fiber is straight and the tilted angle of the fiber is known[76]. A point cloud method, where a low gray-scale threshold was used to retrieve the focused part of the objects, was demonstrated; however, this method is applicable only to straight objects[77]. Recently, an alternative method based on DH was used to automatically characterize an irregular 3D polymeric object. Holograms of a stringy object were recorded using a high-speed DH system. A depth-of-field extended image (DEI) was first obtained by applying an image-fusion algorithm to reconstructed images at different depths[78]. The edge and skeleton of an object are extracted in 2D space[79]. The object was divided into small sections along the skeleton, and a hybrid method[80] was applied to measure the size and 3D location of each section. All sections were stitched together to retrieve the entire object. DH can simplify the 3D visualization of the manipulation process and simultaneously improve the understanding of unstable and asymmetric physical phenomena. Controlling the jetting of liquids and the manipulation of polymers by DH microscopy would extend the potential of direct writing technologies in different fields where high accuracy is required for fabrication procedures.
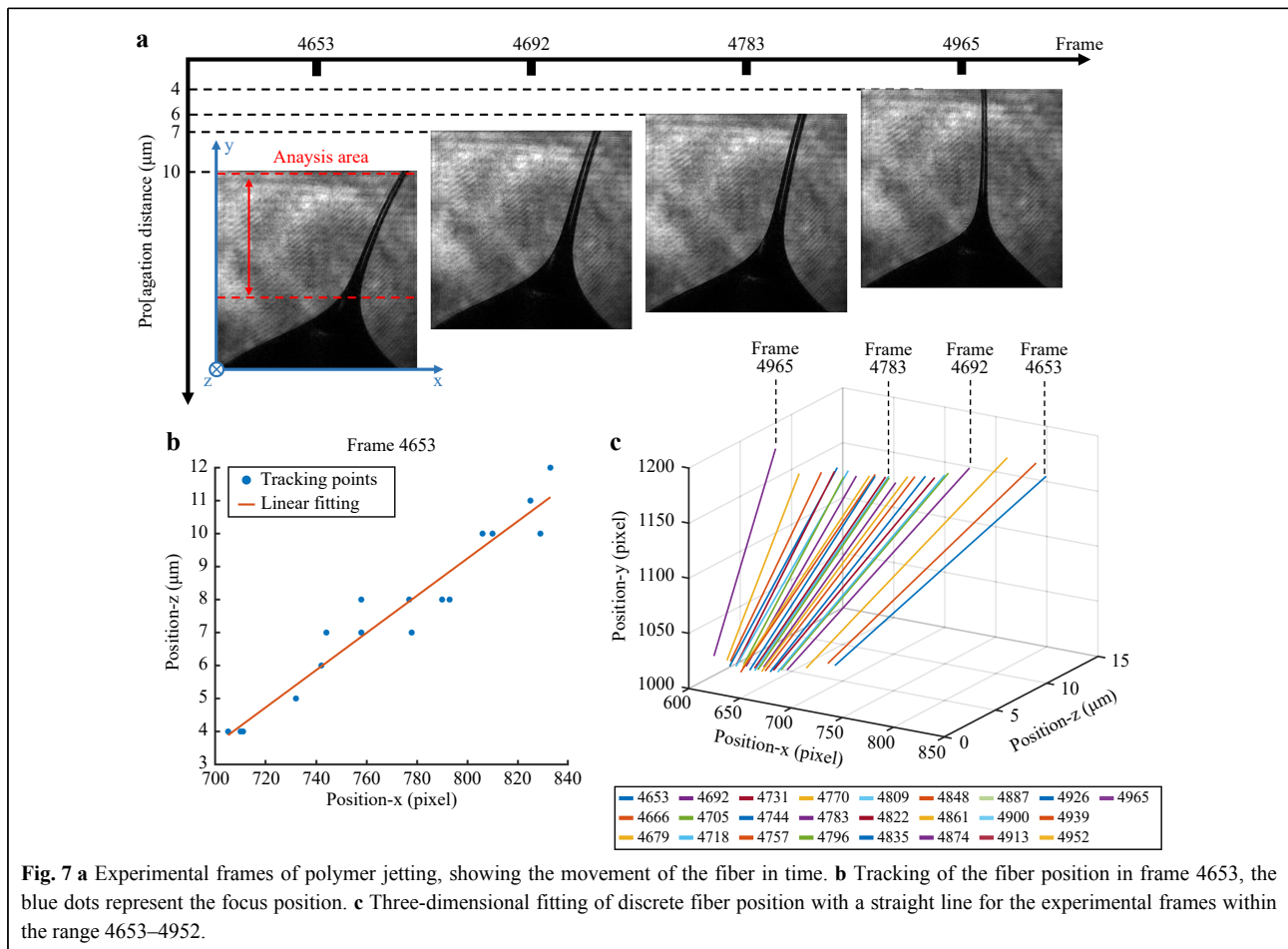
Application of digital holography to monitoring of fibers drawn by electrospinning

The manipulation of polymeric fibers is at the base of an innovative 3D printing fabrication technique, in which the pyroelectric effect is used for direct writing and the fabrication of overprinted scaffolds at the microscale. The printing process was activated directly from a reservoir polymeric drop, avoiding the use of nozzles and external voltages. Under the activation of the tethered pyro-electrospinning (TPES) process, the droplet started to deform, creating an elongated tip from which the fibers were drawn[81,82]. It is very important to follow the 3D movement of the polymeric fiber during the elongation process to achieve high precision in deposition and final resolution of the structure. The DH tool can be improved

for 3D tracking, even in the case of polymer elongation. The results reported below refer to the activation of a polymeric drop of PDMS under the action of the pyroelectric effect. Drop activation can be described by three main steps: drop deformation, cone formation, and cone elongation. During the final step, the polymer fiber could be unstable, and the movement of the final part with the tip could be synchronized with the upper activation zone. Using a conventional visualization line made of a light source, camera, and objective, it would be difficult to follow the evolution in time and space of the polymeric cone. In fact, the cone can move along the vertical axis from the focus of the visualization. Eventually, a tracking technique could enable the reconstruction of more complex and dynamic structures. In particular, under the instability of the pyroelectric effect used for the manipulation of the material, it is possible to observe the activation of Rayleigh instability. Under this condition, beads-on-a-string (BOAS) are generated and can flow over the polymeric fiber. As investigated in our previous work, the elongation, deformation, and eventually the final breakup of

viscoelastic filaments pass through the formation of temporary pearls interconnected by a thin thread, the so-called BOAS structures[83,84]. The evolution in time and space, together with the continuous movement of the fiber and beads flowing on it makes very difficult to observe this process and its characterization.

In this study, a transmissive off-axis holographic recording setup was used to track the movement of polymeric fibers. Owing to the refocusing process of DH, the nonlinear motion process of polymeric fibers can be effectively tracked. Fig. 7 shows the fiber tracking results for 25 frames. Under the action of the pyroelectric effect, PDMS forms fibers that can be recorded, which are so thin that the laser light can pass through them to achieve an effective holographic recording. This significantly improves the accuracy of 3D positioning. However, the numerical diffraction propagation for the entire FoV was difficult to obtain because the fiber showed an increasing trend in the z-axis direction, its top was far away from the recording plane, and its bottom was close to the recording plane. Therefore, we divided the fiber into 17 sub-strips

Fig. 7 a Experimental frames of polymer jetting, showing the movement of the fiber in time. **b** Tracking of the fiber position in frame 4653, the blue dots represent the focus position. **c** Three-dimensional fitting of discrete fiber position with a straight line for the experimental frames within the range 4653–4952.

and performed separate holographic reconstruction and Tamura auto-focusing on each strip to determine the best z-axis position. In Fig. 7b, we report the result of frame 4653 as an example, where the blue dots indicate the focal position of each band. The feature correlation recognition method was used to track the x-axis position of the fiber. Here, the y-axis position of the fiber is the absolute position, and the x- and z-axes are the measurement positions. Therefore, the spatial coordinate distribution has a certain discrete type under an overall uniform trend. To facilitate the identification, we fitted the 3D discrete fiber position identification points with a straight line for all steps of fiber movement, as shown in Fig. 7c.

Application of digital holography to monitoring of beads-on-a-string over fiber drawn by EHD
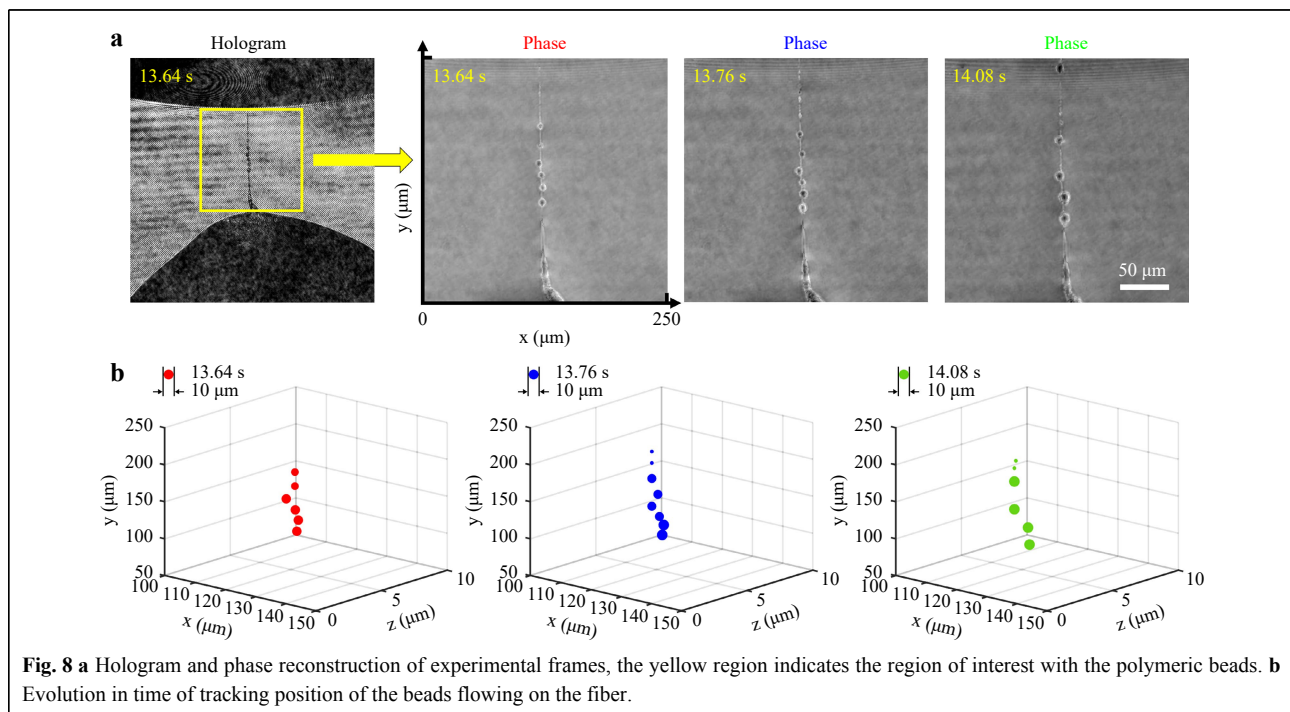
DH also enables us to accurately locate BOAS structures over thin polymeric fibers. As shown in Fig. 8, we selected three frames from a series of BOAS generation processes to reconstruct the position and size of each bead. The spatial location and size of each bead are shown in Fig. 8b. Here, multi-steps diffraction propagation and stripes reconstruction process were used to extract the bead information. Furthermore, in the 2D phase as shown in Fig. 8a, which is reconstructed by a uniform propagation distance, we could see that the beads were arranged vertically on the fiber, but after holographic 3D positioning, the size and spatial position of each bead,
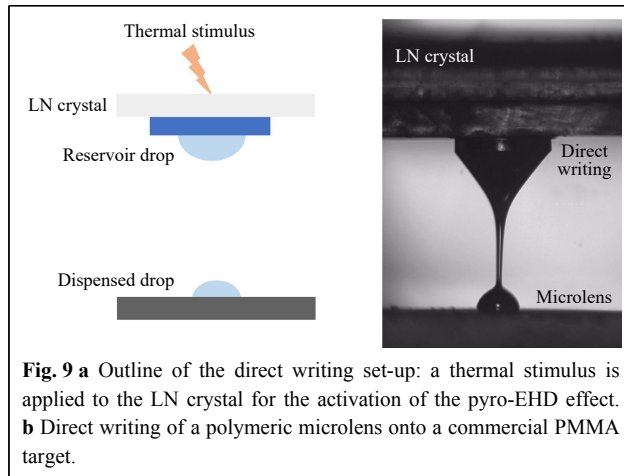
including z position, could be retrieved, providing important data for further quantitative analysis.

Digital holography and characterization of polymeric lenses printed by EDH ink jet printing

The process of cone formation at the base of the polymer elongation described in the previous section can also be adopted for the jetting of the polymeric drop. In particular, once the electric charges accumulated on the tip of the polymeric cone overcome the surface charges of the material, small volumes can be dispensed and collected onto a commercial target. In this configuration, the starting reservoir polymeric drop was deposited on a pillar base, while the pyroelectric crystal was mounted over the coverslip upon which the drop was supported, and was heated locally together with the base droplet, thus allowing the generation of pyroelectric surface charges on the crystal. The liquid droplet started to deform under the action of a sufficiently strong electric field, and was released from the conical tip microdroplets onto a moving substrate. By controlling the starting volume, contact angle of the substrate, and by selecting the polymer of interest, droplets of different geometries and volumes could be dispensed by direct writing (see Fig. 9).

Once cured, the polymeric structures could be used as optical microlenses, and interferometric characterization based on DH microscopy was carried out to evaluate the optical aberrations of the microstructures and their

Fig. 8 a Hologram and phase reconstruction of experimental frames, the yellow region indicates the region of interest with the polymeric beads. **b** Evolution in time of tracking position of the beads flowing on the fiber.

Fig. 9 a Outline of the direct writing set-up: a thermal stimulus is applied to the LN crystal for the activation of the pyro-EHD effect. **b** Direct writing of a polymeric microlens onto a commercial PMMA target.

focusing properties[85,86]. The optical setup consisted of a classical Mach-Zehnder interferometer in the transmission configuration, as shown in Fig. 10.

The beam emitted by a continuous-wave (CW) laser with wavelength $\lambda = 632.8$ nm is first split into two parts, constituting the reference and the object arm of the interferometer. Both encounter a 5 × microscope objective on their path toward the sensor (a 1024 × 1024 CCD camera with pixel pitch $\Delta x = \Delta y = 4.4$ μm). The object beam is directed toward the microfluidic chip where a sample microlens is deposited and it then recombines to the reference in the acquisition plane to produce an interference pattern. Once the hologram is recorded, numerical propagation provides the object complex field in any plane along the optical axis z, from which the intensity and phase distributions of the optical wavefield transmitted
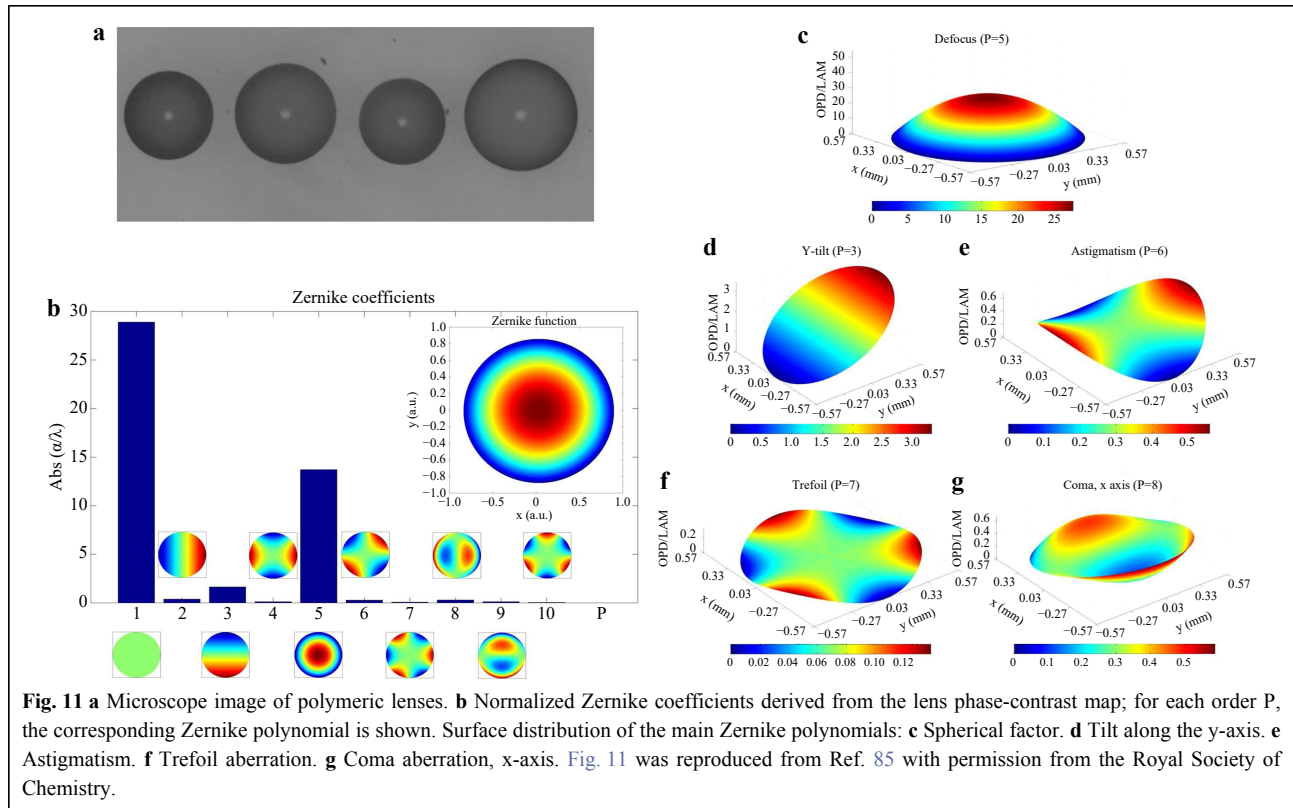

Fig. 10 Mach-Zehnder interferometer in transmission configuration used for the characterization of the polymeric lens fabricated on the microfluidic channel by direct writing. Fig. 10 was reproduced from Ref. 85 with permission from the Royal Society of Chemistry.
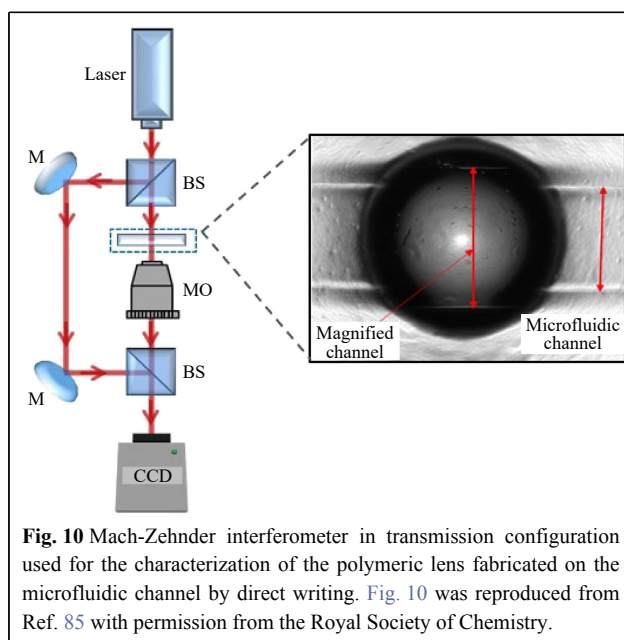
by the sample can be extracted[87]. A double-exposure method was adopted to compensate for the aberrations of the optical components in the setup, as well as the phase delay introduced owing to the passage of the object beam through the chip. Hence, the recovered phase-contrast map directly yields information on the optical behavior of the lens. The analysis was performed by exploiting the Zernike fitting to evaluate the contributions of the defocus and other aberration terms. The results of the Zernike analysis are shown in Fig. 11.

Digital Holography for characterizing self-assembled liquid microlenses

The pyroelectric effect has also been investigated to change the wettability of micro-engineered surfaces. In particular, the wettability of LN crystals is patterned by inducing a pyroelectric effect on the domain-engineered samples. As previously mentioned, this technique enables wettability patterning to be achieved by an electrode-less configuration, in contrast with conventional electro-wetting (EW) experiments. In fact, the surface charges inducing this effect are pyroelectrically generated and spatially modulated by the domain grating. A micro-array of thousands of sessile droplets is obtained on a single chip, and using a DH apparatus, it is possible to characterize such microstructures, demonstrating their optical quality as microlenses.
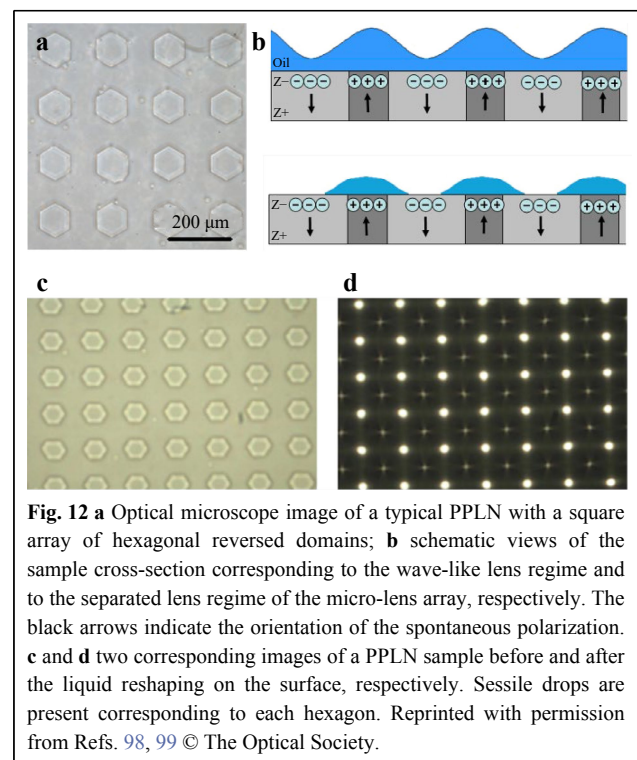
Wettability patterning at solid surfaces is an important aspect for different applications, such as the self-assembly and alignment of particles, as well as for all integrated microfluidic and optofluidic systems where liquid actuation is fundamental[88–91]. EW allows the alteration of the wetting properties of a substrate by means of free electrical charges[92,93]. Among all the application fields, EW has been demonstrated to be a key technology for realizing liquid lenses[94,95]. Usually, EW-based experiments require complex electrode geometries to actuate and control the surface wettability. Therefore, the possibility to pattern surface wettability by activating specific properties of the material without using external electrodes is desirable.

In this section, it is shown that by activating the pyroelectric effect in periodically poled LN (PPLN) substrates, it is possible to pattern and control the surface wettability without the need for external electrodes and circuits. This technique can be used to generate an array of sessile droplets according to the reversed domain structure of the PPLN substrate. LN is a rhombohedral crystal that exhibits pyroelectricity at certain condition. The spontaneous polarization, P_S, changes according to $P_i = \xi_i \Delta T$, where ξ_i is the pyroelectric coefficient and ΔT is the temperature variation. At equilibrium, all P_S in the

Fig. 11 a Microscope image of polymeric lenses. **b** Normalized Zernike coefficients derived from the lens phase-contrast map; for each order P, the corresponding Zernike polynomial is shown. Surface distribution of the main Zernike polynomials: **c** Spherical factor. **d** Tilt along the y-axis. **e** Astigmatism. **f** Trefoil aberration. **g** Coma aberration, x-axis. Fig. 11 was reproduced from Ref. 85 with permission from the Royal Society of Chemistry.

crystal are fully screened by the external screening charge, and no electric field exists[96]. A temperature change modifies P_S, and consequently, such equilibrium is perturbed, causing a lack or excess of surface charge, thus generating a high electric field. The spontaneous polarization of LN was inverted by photolithography and electric field poling to obtain a periodic square array of hexagonal reversed domains. Fig. 12a shows an image of the PPLN crystal. Fig. 12b shows a schematic of the patterning effect induced by the temperature change. A thin layer of an oily substance was spread onto the crystal surface. The sample was made of a crystal substrate, and the oil film was heated and then cooled down, the whole explored range of temperatures is from 25 to 100 °C[97]. All the reported results were obtained using carboxylic acid (pentanoic acid - $C_5H_{10}O_2$) as the oily substance spread onto the z-cut $LiNbO_3$ substrates. The liquid film experienced only a smooth shape modification during heating, with the liquid-air interface exhibiting a wave-like (WLR) profile following the geometry of the domain array (top of Fig. 12b). Conversely, pronounced wettability patterning is observed during cooling, which is called the separated lens regime (SLR), as shown in the bottom part of Fig. 12b, when the liquid film starts to break in different regions, forming isolated sessile droplets. The final result consists of an array of sessile droplets that follow the

geometry of the PPLN domain structure (see the bottom part of Fig. 12d).

Fig. 12 a Optical microscope image of a typical PPLN with a square array of hexagonal reversed domains; **b** schematic views of the sample cross-section corresponding to the wave-like lens regime and to the separated lens regime of the micro-lens array, respectively. The black arrows indicate the orientation of the spontaneous polarization. **c** and **d** two corresponding images of a PPLN sample before and after the liquid reshaping on the surface, respectively. Sessile drops are present corresponding to each hexagon. Reprinted with permission from Refs. 98, 99 © The Optical Society.

Both regimes, i.e., WLR and SLR, were investigated using a DH microscope set-up to characterize the focusing behavior and optical aberrations of the microlenses. Fig. 13a shows a schematic view of the interferometric apparatus used for the measurements based on the Mach-Zehnder interferometer. The calculated wrapped phase map of the lens microarray is shown in Fig. 13b, and after applying an unwrapping algorithm, the continuous-phase image for the microlens array is retrieved, as shown in Fig. 13c.

The temperature of the thermo-controlled plate under the sample was varied at a rate of 10 °C/min, and it was controlled with an accuracy of 0.1 °C. Interferometric characterization was performed by registering the temperature value for each digital hologram captured during thermal treatment. Two different types of analyses were carried out to evaluate the temperature dependence of the focal length and optical aberrations of the lenses, thus characterizing both the tunability and optical performance of the device. The temperature dependence of the focal length was independently investigated during the cooling and heating treatments. The aberrations of the lenses were evaluated through a deeper analysis of the wavefronts transmitted by the lenses themselves, and this was done by exploiting the Zernike fitting[98–101].

The wrapped phase maps exhibit different behaviors in the case of heating and cooling. When the temperature increases, oil shaping occurs only up to a temperature value of approximately 65 °C, and consequently, the number of fringes increases. After this temperature, the lens shape stabilized. Conversely, during the cooling process, the number of fringes increased during the whole process. An unwrapping numerical procedure was applied to phase mode 2π to measure the real phase distribution of the wavefront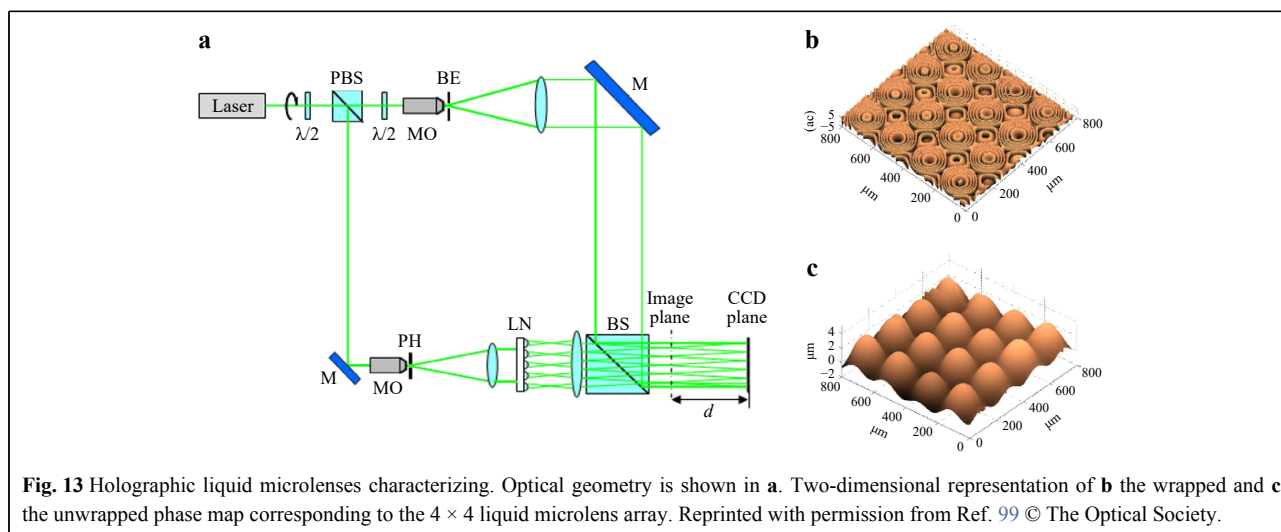. Subsequently, a one-dimensional (1D) fitting procedure was performed to evaluate the focal length of each microlens in the array. Fig. 14a, b show the experimental and fitted profiles of the unwrapped phase corresponding to the two different processes. The focal length trend vs. temperature variation is reported in Fig. 14c, d for both the heating and cooling experiments.

The optical behaviors of the microlenses were also characterized in terms of optical aberrations by applying a 2D fitting algorithm to digital holograms of a 4 × 4 lens array acquired during stationary conditions, that is, when the number of fringes is stable in the wrapped phase distribution, while the fitting procedure was performed for each lens of the array and for lenses of several arrays at different time instants. The function used for the fitting process is a linear combination of Zernike polynomials by considering the coefficients for the tilt, astigmatism, defocus, and third-order spherical aberration terms. The coma and higher-order coefficients were neglected because some orders of magnitude were minor.

Fig. 15 shows the surface distribution of each polynomial employed for Zernike fitting, and it enables us to visually compare the focus term with the other terms that describe the wavefront curvature. The main term is the defocus term, which allows the state of the quality of such a microstructure, and the spherical aberration term has a quite high value because the curvature changes from convex to concave between two adjacent microlenses.

Application of digital holography to the characterization of other printed micro-structures

DH can be used to characterize microfluidic structures. In fact, the direct printing previously described could be implemented for the fabrication of high-resolution microchannels with transversal sizes ranging from several
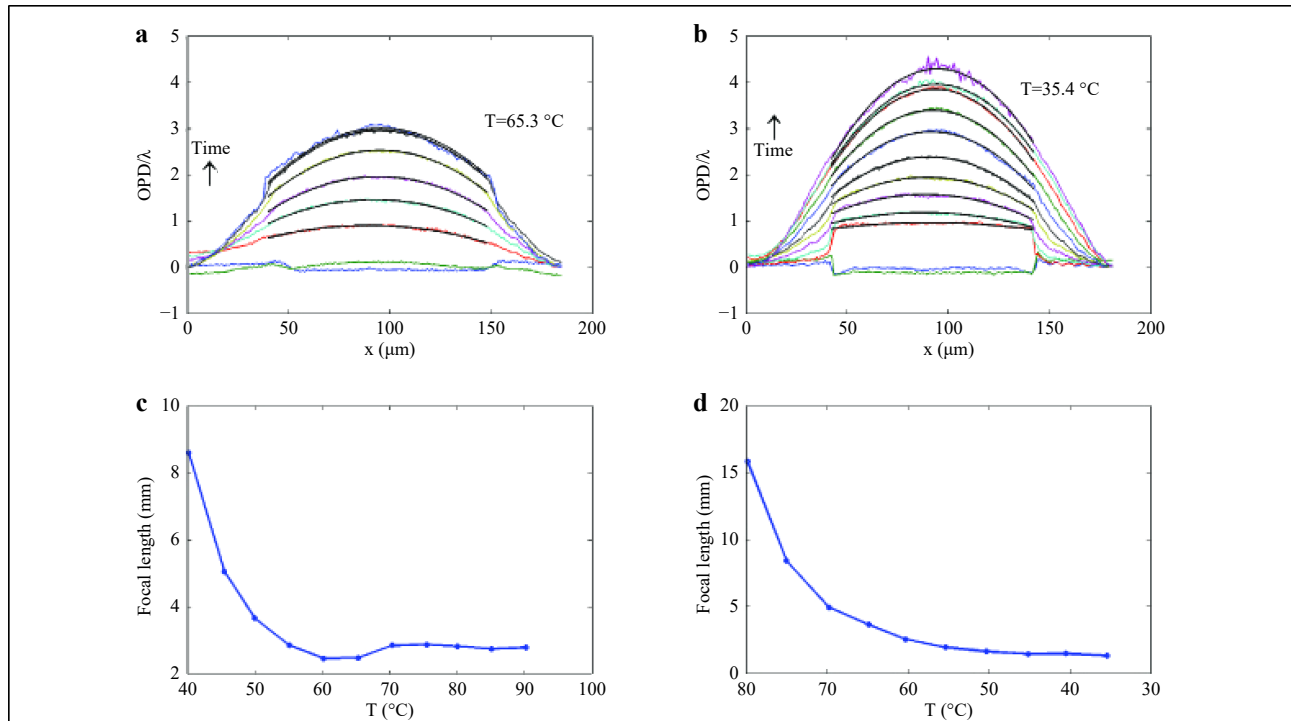

Fig. 13 Holographic liquid microlenses characterizing. Optical geometry is shown in **a**. Two-dimensional representation of **b** the wrapped and **c** the unwrapped phase map corresponding to the 4 × 4 liquid microlens array. Reprinted with permission from Ref. 99 © The Optical Society.

Fig. 14 Experimental and fitted profiles of the unwrapped phase distribution corresponding to **a** the heating and **b** cooling process; **c**, **d** focal length variation as a function of temperature in case of the heating and the cooling process. Reprinted with permission from Ref. 99 © The Optical Society.
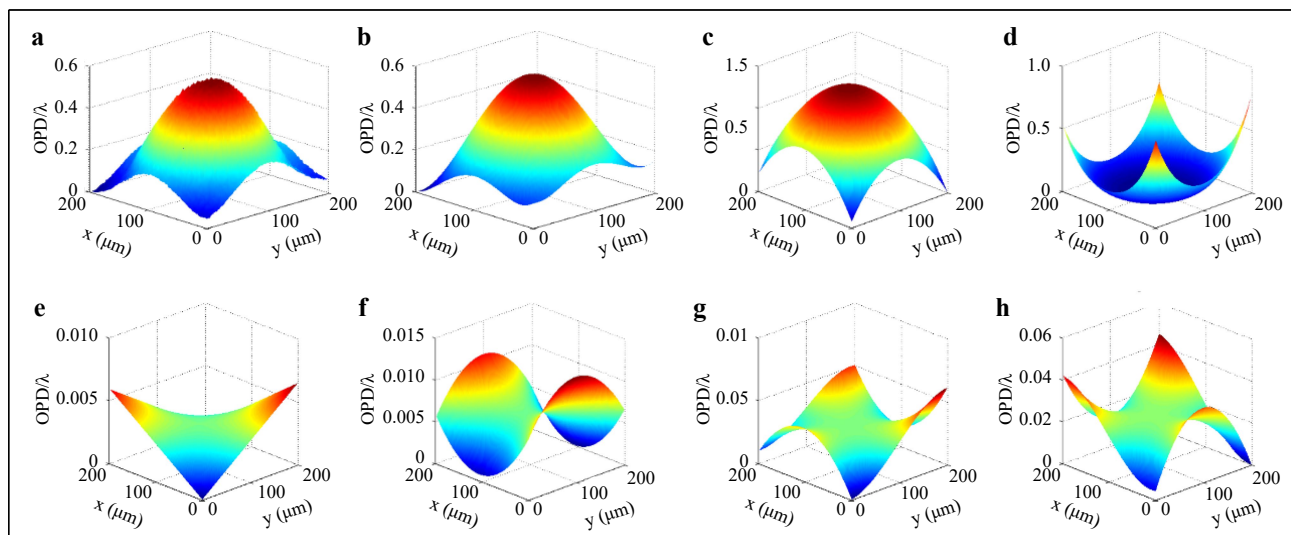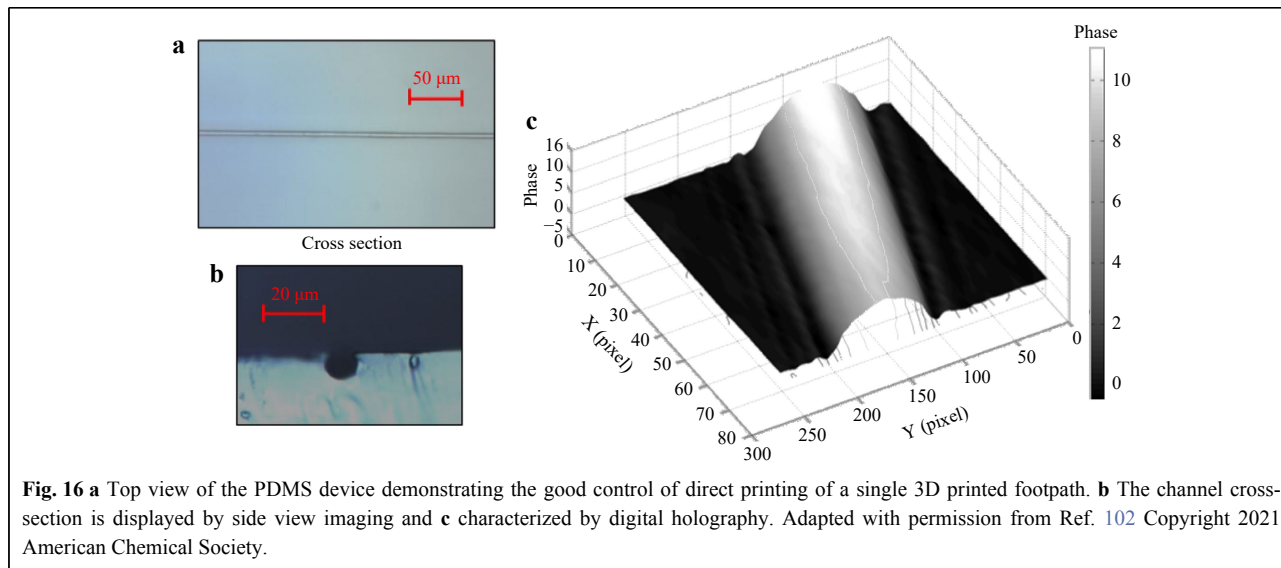

Fig. 15 a Measured phase distribution and **b** corresponding Zernike fitted surface; **c** surface distribution of the focus term, **d** the third order spherical aberration, **e** the astigmatism at 45° term, **f** the astigmatism at 90°, **g** the triangular astigmatism on the x base, **h** the triangular astigmatism on the y base. Reprinted with permission from Ref. 99 © The Optical Society.

hundreds of nanometers to hundreds of microns[76]. The printing resolution that has been demonstrated is well below the resolution limit of standard methods, even in the case of processing biocompatible and biodegradable materials, so the final devices are useful candidates for biological analysis because of their intrinsic absence of toxicity and immunogenicity (Fig. 16a, b). In the case of a straight channel (length 1.5 cm and diameter limited to approximately 2 μm), interferometric characterization based on DH microscopy was carried out to evaluate the

Fig. 16 a Top view of the PDMS device demonstrating the good control of direct printing of a single 3D printed footpath. **b** The channel cross-section is displayed by side view imaging and **c** characterized by digital holography. Adapted with permission from Ref. 102 Copyright 2021 American Chemical Society.
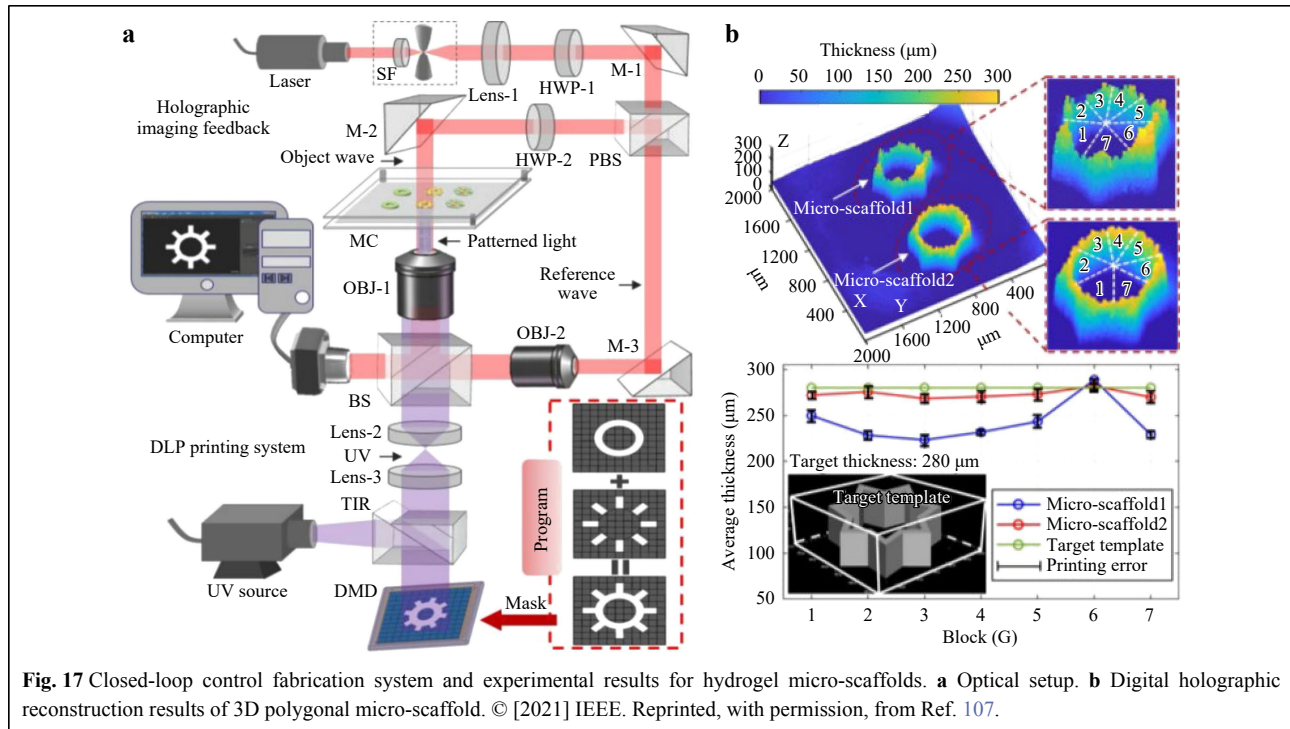
morphology and quality of the footpath finish, as shown in Fig. 16c. The cross-section of the channel is cylindrical, showing the 3D core of the pyro-electrospun microfiber.

Closed-loop fabrication of micro-scaffold combination of digital light processing and digital holography

Currently, the field of artificial biological tissues represents an area of much research interest, and applications range from artificial skin to liver lobules. Similar to the way that a complete LEGO set is made up of bricks, artificial biological tissues can be assembled on the cellular micro-scaffolds. These micro/nanoscale scaffolds are the navigators of cell growth; they can guide the cells' behavior by their spatially heterogeneous architecture, and further influence the functional expression of the engineered tissues directly[103]. Researchers have developed different micro/nano scaffold fabrication methods to advance techniques used when manufacturing different artificial tissues[104–106]. The possibility of monitoring in real-time and in situ high-resolution fabrication processes through accurate characterization remains a significant challenge. Recently, a closed-loop control system for the fabrication of high-fidelity micro-scaffolds was proposed[107]. A combination of digital light processing (DLP) and digital holographic microscopy (DHM) has been used to precisely manufacture cell-encapsulated hydrogel micro-scaffolds under real-time monitoring. Poly(ethylene glycol) diacrylate (PEGDA) and gelatin methacrylate (GelMA) hydrogels were used as experimental materials to fabricate micro-scaffolds using the DLP system. Meanwhile, the 3D imaging capability of DH provided support for the quantitative monitoring of

liquid-solid conversion by ultraviolet (UV) light. Fig. 17a shows the proposed set-up used for the holographic feedback-based photocuring system. Herein, DLP guided the fabrication of hydrogels under UV light, while DHM furnished quantitative observation of the forming material. The UV beam, which is modulated by a digital micro-mirror device (DMD), illuminated the hydrogel in a designed manner. Meanwhile, the hydrogel was processed by the UV beam, and it was also irradiated by the laser beam from the DH setup. The object beam carrying its information interferes with the reference beam on the camera screen to form a digitally recorded hologram.

The experimental results are shown in Fig. 17b. To verify the calibration capability of the DH for the fabrication process, comparative experiments were conducted. Herein, the first micro-scaffold (test 1) was fabricated using the DLP printing system without DH monitoring, whereas the second micro-scaffold (test 2) was fabricated under the feedback control of the DHM. Each micro-scaffold was divided into seven blocks by dashed lines to fit the average thickness of each block. The expected thickness of the fabrication template was 280 μm, as indicated by the green line in the plot. Comparing the results, micro-scaffold 2 exhibited smoother surface topography. In general, the fluctuation range of the fitted curve for micro-scaffold 1 was 65.4 μm, which was larger than the fluctuation range obtained for micro-scaffold 2, which was 12.7 μm. From the cross-sectional view, it can be more clearly observed that DHM played a key role in improving the manufacturing accuracy and stability of the DLP system. Using the same approach, the relationship between the Young's modulus and exposure duration was investigated. The above experimental results effectively

Fig. 17 Closed-loop control fabrication system and experimental results for hydrogel micro-scaffolds. **a** Optical setup. **b** Digital holographic reconstruction results of 3D polygonal micro-scaffold. © [2021] IEEE. Reprinted, with permission, from Ref. 107.

prove the positive effect of DHM on hydrogel micro-scaffold fabrication for constructing a heterogeneous architecture inside a single integrated micro-scaffold. The use of DHM as a closed-loop control method to improve the fabrication accuracy will be an important topic in the near future, especially for the processing of biological materials. The organic combination of transmissive, micron-level, real-time, and 3D imaging in DHM is expected to lead to the development of a good tool for the fast and high-precision fabrication of artificial biological tissues.
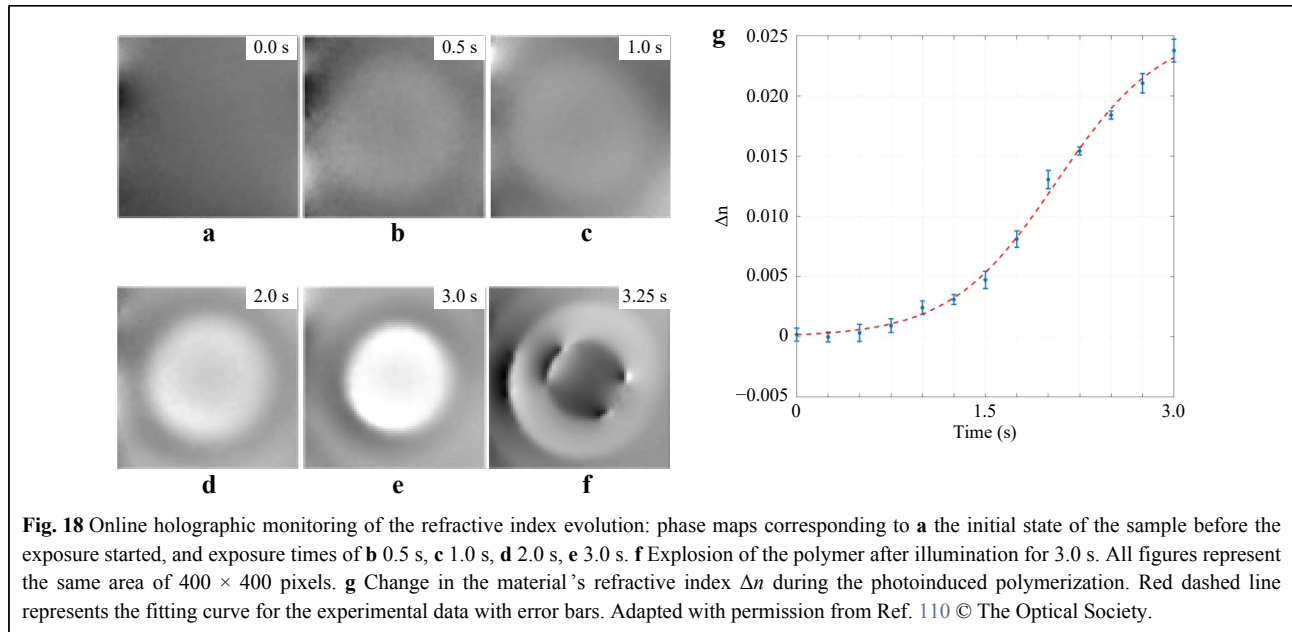
Assisting two-photon polymerization fabrication process by digital holography

The increase in miniaturization from medical engineering to consumer electronics requires the development of advanced fabrication methods. Recently, 3D printing was proposed for the fabrication of micro-optics and miniaturization of spectroscopic compact and integrated measurement systems[108]. However, among the existing manufacturing methods, 3D lithography by two-photon polymerization shows intriguing functionalities for printing complex 3D structures of different geometries, including curvilinear features, with a submicrometer resolution[109]. Recently, there has been increased attention on the characterization of samples fabricated by such technology. In fact, it is challenging to address specific goals for two-photon lithography and even more useful

manufacturing approaches, such as the non-destructive online monitoring of photoinduced polymerization. Holographic monitoring of photopolymerization dynamics has recently been demonstrated by characterizing the evolution of the photoresist RI during the photopolymerization process[110,111], please see Fig. 18.

Monitoring creation of surface relief gratings using digital holography

Complex surface relief patterns can be manufactured by the light-induced surface structuring of azobenzene-containing films. Such relief patterns, which have different heights and topography patterns, are difficult to achieve using conventional lithography systems, and understanding their formation dynamics and response to different types of light irradiation is still an open task. Recently, DH has been explored to investigate the manufacturing processes. In particular, significant results have been reported on the potential for the development of holographic tools that can write the desired surface relief grating (SRG) structures, and furnish the quasi real-time and in-situ monitoring of the process. In one configuration, a Lloyds interferometer was used to create the SRG pattern, while a DH microscope, working with a He-Ne laser emitting at 632.8 nm, was used to monitor its formation and dynamic evolution[112]. In a more recent paper, the interference pattern for SRG writing was monitored using a DHM operating with a 488-nm light input and a polarization-maintaining

Fig. 18 Online holographic monitoring of the refractive index evolution: phase maps corresponding to **a** the initial state of the sample before the exposure started, and exposure times of **b** 0.5 s, **c** 1.0 s, **d** 2.0 s, **e** 3.0 s. **f** Explosion of the polymer after illumination for 3.0 s. All figures represent the same area of 400 × 400 pixels. **g** Change in the material's refractive index Δn during the photoinduced polymerization. Red dashed line represents the fitting curve for the experimental data with error bars. Adapted with permission from Ref. 110 © The Optical Society.

fiber[113]. The results reported in this paper prove that DH can provide an optimal measuring instrument for monitoring the formation of SRG patterns. The experimental setup and results are shown in Fig. 19.

Toward the investigation of rheology, stress monitoring, and particle tracking by digital holography
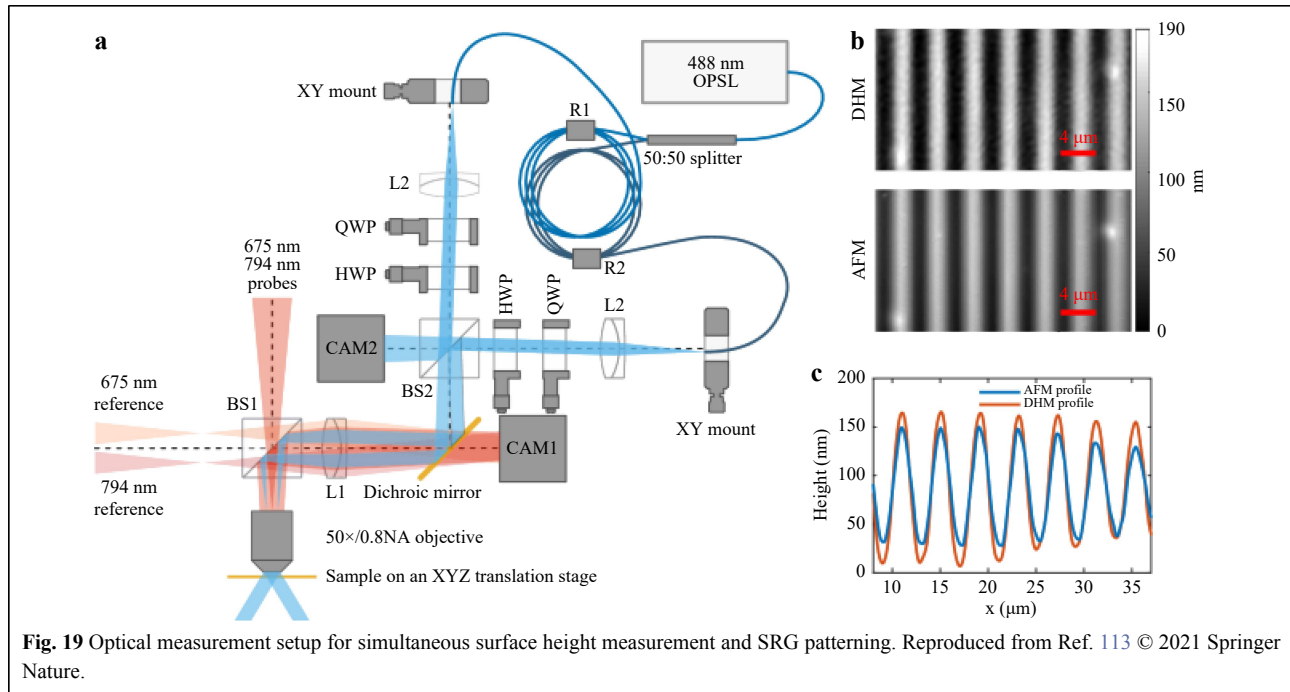
Stress monitoring in soft materials using digital holography

In the pioneering era of DH, many applications have been explored for quantitative analysis and to obtain accurate measurements in transparent materials. The analysis of liquids, gases, plasma, and photoelastic materials has been demonstrated. In fact, owing to the intrinsic features of holographic methods, it was possible to study stress formation in photopolymers during the live recording of holograms. A recent paper[114] demonstrated that it is possible to detect and retrieve stress formation during the recording and bleaching of photopolymer holograms as a result of the distortion of the internal diffractive structure. This is particularly important in the case of holographic solar concentrators or other holographic optical elements that must meet stringent specifications. DH measured the stress formation in photopolymers during hologram acquisition by recording many holograms at successive exposure time intervals.

Another example of the capability of DH to measure deformation was presented in Ref. 115. In this research, it was shown that the deformation of cylindrical nanostructures made of silica aerogels can be analyzed using DH. In particular, two-beam phase-shifting digital holographic interferometry was applied to investigate in-plane displacements. While the structures under investigation were mechanically loaded with various loads from the top surface, phase-shifted holograms of the silica aerogels with and without deformation were acquired using a CCD camera. Reconstruction of the complex amplitude of aerogel samples using the Fresnel diffraction integral was adopted to analyze the reordered holograms. In-plane displacements were obtained from the phase distribution of the deformed aerogels by measuring the change in the two-phase distributions, enabling the observation of their elastic behavior. The deformation of silica aerogels was observed within the range of 0.02058 cm to 0.0017 cm, corresponding to an increase in bulk density from 0.01742 gm cc^{-1} to 0.1952 gm cc^{-1}.

A further example of the application of DH in measuring mechanical properties is the investigation of the Young's modulus of polyacrylamide gels[116]. DH is shown to be a convenient technique for measuring the Young's modulus of soft materials for cellular adhesion. The interaction between an elastic substrate and adherent cells plays a key role in regulating functions and behaviors in the concentration, migration, and proliferation of the cells. Polyacrylamide (PAA) is a soft polymeric gel and a flexible substrate with specific mechanical properties commonly used for testing the mechanical properties of cells. However, to quantitatively measure the stress induced by cells, it is necessary to determine their mechanical response with high accuracy. The accurate

Fig. 19 Optical measurement setup for simultaneous surface height measurement and SRG patterning. Reproduced from Ref. 113 © 2021 Springer Nature.

measurement of the Young's modulus can be achieved through DH by retrieving the optical phase of the light transmitted through the transparent gel.

Investigating microfluidic rheology and liquid-solid interfaces using digital holography

To the best of our knowledge, Lorenz-Mie analysis has been widely used in in-line DHM to track and measure colloidal particles[117], which is also known as holographic particle characterization (HPC). Owing to the Lorenz-Mie theory of light scattering, the 3D tracking of particles with nanometer precision while simultaneously measuring each sphere's radius and refractive index could be achieved. This technique can be used not only for a single particle but also for measuring multiple colloidal particles, as reported by Fung et al.[118]; in this study, up to six colloidal spheres were accurately modeled based on superposition solutions. In the past decade, HPC with Lorenz-Mie analysis has been applied to different areas of colloidal particles. In 2014, Krishnatreya et al. successfully measured the Boltzmann constant of a single particle[119], which means that individual colloidal particles can be tracked over large distances with high precision. In 2017, Cheong et al. applied HPC to colloidal particles in turbid media[120], for the first time verifying its applicability in translucent media. In addition to the above applications, HPC can be used to guide the development of synthesis protocols for colloidal particles[121]. The monodisperse TPM sphere fabrication process was examined by HPC to study

the influence of protocol choices on the size and refractive index.

In a recent study, DH microscopy in conjunction with particle tracking velocimetry (PTV) was implemented to measure microfluidic shear rheology and the wall slip of viscoelastic fluids[122,123]. The technique involves introducing non-deformable microparticles into the fluid, recording the holograms, and identifying the particle centroid locations in 3D with a digital reconstruction of the particle scattering field for an imposed driving pressure. Starting from the PTV, it is possible to retrieve the velocity and characterize the shear rheology of the viscoelastic fluids. Then, using a small sample volume (approximately 20 μl), it was possible to characterize the shear rheology of viscoelastic fluids across a wide range of shear rates. The results were compared with those of simulations and classical macrorheometry. Moreover, a recent study used DH to monitor surface slippage to investigate microparticle sedimentation[124]. Understanding the behavior of microparticle sedimentation in fluids is of fundamental importance for many industrial processes and natural phenomena. Digital holographic microscopy was used to measure the effect of the proximity of a flat microfluidic chamber wall on the sedimentation of colloidal microspheres. The numerical refocusing feature of DH was employed to track multiple particles instantaneously, obtaining quantitative images of the samples. By analyzing the 3D paths and speeds of multiple sedimentation microparticles, it was shown that the proximity to flat walls

of higher slip lengths causes faster sedimentation. This effect was driven by the ratio of the particle size to the slip length and its distance from the walls. Moreover, the dependence of the 3D trajectories on the internal coatings provided to the chamber walls was also retrieved. In Fig. 20, the paths followed by different microparticles are shown, as they are retrieved by DHM.

Holographic technology has a wide range of applications in microfluidic imaging. A typical example is the application of holographic particle image velocimetry (HPIV) to track particles in fluids[125,126], especially when the particle density is high and the 3D spatial distribution is complex. Here, HPIV technology based on an off-axis DH setup was used to track the particles inside the thin films and realize the tracking of large-scale 3D liquid flow[36]. As the twin technology of in-line DH with Lorenz-Mie analysis, off-axis HPIV focuses on particle tracking for undefined spaces with ultralong-distance movement.

In this experiment, particles with a diameter of 10 μm were injected into the PA solution, which moved with the film during the pumping of the bubble. Fig. 21 shows the trajectories of the three particles, from which the gravitational drainage process of the thin film can be clearly observed. The most notable among them is particle A, which first raised gradually with the film and then quickly moved to the edge with a decrease in height. These datasets can be used to better understand the liquid flow movement process on the surface of the film and convert complicated liquid flow tracking into simple particle tracking. In fact, this technology can be applied in many
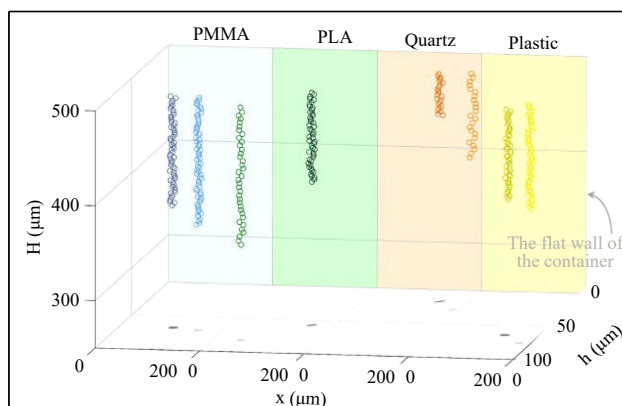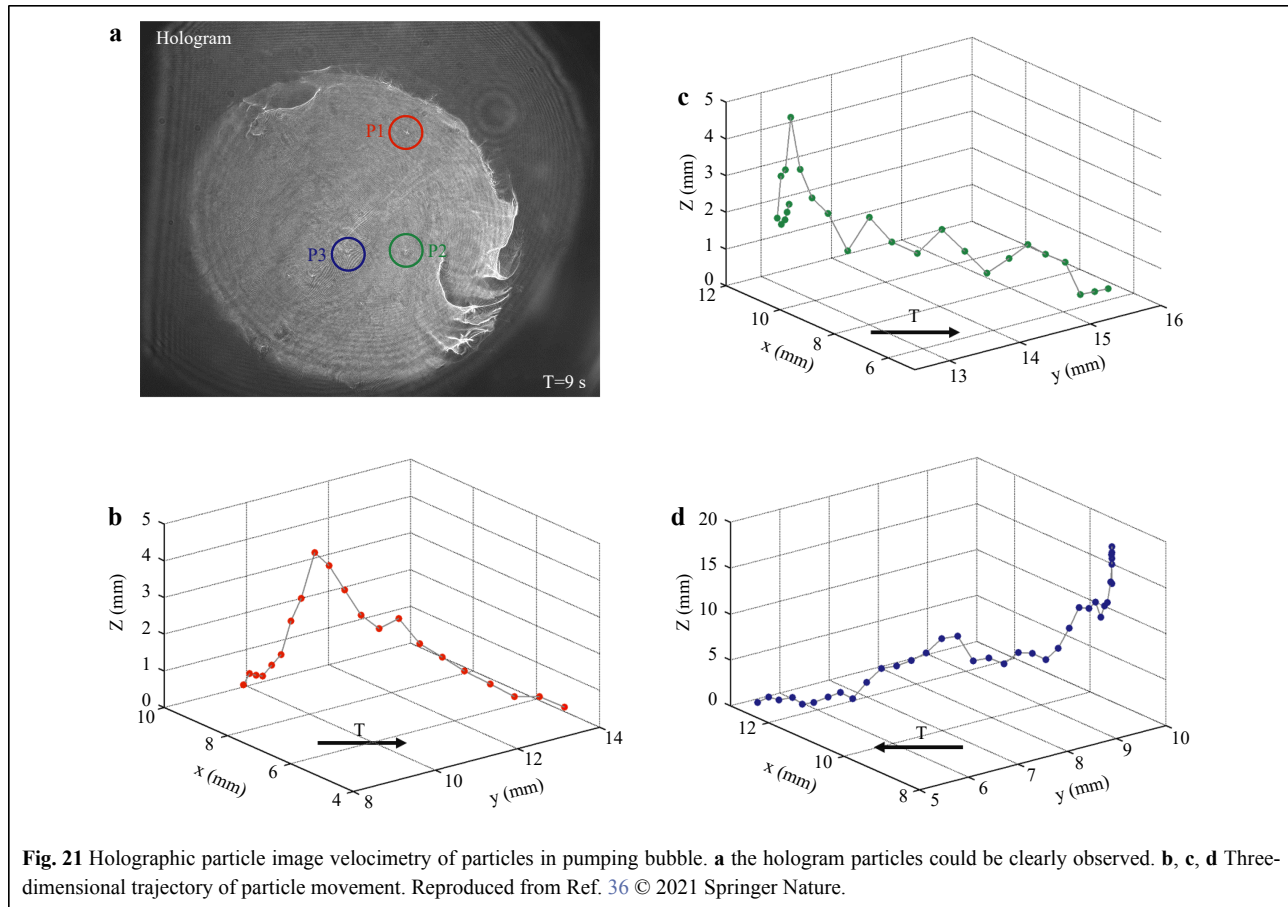

Fig. 20 3D trajectories of several polystyrene micro-particles at different distances from the flat wall of the container within 5 s and in different levels of hydrophobicity wall effects (PMMA, PLA, Quartz, Plastic). The different materials and the sedimenting micro-particles near them are shown in different colors. The different colored circles show the sedimenting micro-particle distances to the flat wall; lighter colors indicate farther ones. Reproduced from Ref. 124 © 2021 Springer Nature.

experiments on film motion processes in the study of membrane gravitational drainage and rupture processes.

Application of deep learning to soft matter holographic measurement

The integration of deep learning with DH imaging is an emerging and widely studied topic. In the digital holographic morphology of soft matter, deep learning can also be used to enhance recording and numerical reconstruction processes, especially for colloid aggregation[127]. In 2020, Altman et al. proposed a method for characterizing and tracking colloids holographically (CATCH) in colloidal dispersions[128]. In this study, in-line holograms of colloids were studied using a neural network to acquire the properties of the particles. Although the CATCH output did not achieve the full precision of the conventional Lorenz-Mie analysis, it successfully provided approximate results in a shorter time, providing a new solution for the analysis of the colloidal dynamics process. In 2021, Midtvedt et al. used deep learning to enhance the optical characterization of subwavelength particles[129]. A neural network was applied to link the reconstructed results with the real radius and refractive index of individual subwavelength particles. In this case, the holographic scattering patterns of single particles contain sufficient information to reveal the subwavelength size and the precise refractive index. As a result, the aggregation kinetics of a sample consisting of polystyrene nanoparticles were monitored by combining DH and deep learning without prior knowledge of the physical properties of the surrounding medium. Furthermore, this method could be extended to other application scenarios; for example, tracking the movement of aggregates in special microfluidic channels, and it will open new possibilities for characterizing particle interactions and properties[130]. Neural networks can also be used to improve the accuracy of phase reconstruction for the morphology of time-varying objects, such as fluids and soft matter. Lu et al. proposed an Ynet-ConvLSTM network for extracting phase information during dynamic holographic imaging[131]. The time-related information in the hologram sequence was learned by the neural network, and it was then used to improve the reconstruction accuracy and suppress the background noise. The author implemented the proposed method on quantitative holographic droplet alcohol evaporation imaging, and a comparison between different reconstruction methods was presented. From the results obtained, the phase information obtained by the Ynet-ConvLSTM network reveals higher precise object information compared with the results obtained from the conventional Unet method and two-step phase-shifting

Fig. 21 Holographic particle image velocimetry of particles in pumping bubble. **a** the hologram particles could be clearly observed. **b**, **c**, **d** Three-dimensional trajectory of particle movement. Reproduced from Ref. 36 © 2021 Springer Nature.

algorithm. Through the combination of conventional holographic recording and deep learning reconstruction, phase extraction under a neural network will challenge the conventional numerical diffraction reconstruction process to achieve dynamic high-precision low-noise imaging. In the future, the combination of the DH method based on the deep learning reconstruction process and wavefront shaping[132] may create more possibilities and expand the application scenarios of holographic soft-matter measurement.

Conclusions

We have presented, reviewed, and extensively discussed how DH can be a suitable metrology tool for use in a variety of challenging cases dealing with soft matter, that is, with liquid/polymer matter and fast dynamically evolving processes such as inkjet printing. DH can successfully provide engineering solutions for many applications and basic scientific questions. Even though this review is not exhaustive, we believe that we have reported the most significant cases in which such measurement techniques can be effectively applied to soft matter. We have intentionally excluded "biological

matter", as it is outside the scope of this review. In particular, we reported on the applications of DH measurement for different types of soft matter, such as thin films, EHD drawn fibers, polymeric lenses, micro-channels, hydrogel micro-scaffolds, photoresists, surface relief gratings, and particles. Table 1 lists the implementation conditions and parameters of the relevant measurements, where we identified the optimal measurement approaches for different materials/processes.

For most transparent soft matter, DH is one of the best candidates for implementing measurements. Among them, the special case is for ultra-thin liquid films, meaning liquid films with an average thickness of less than 1 μm; WLI will be the best method in theory because it has excellent resolution for smooth sub-micron thickness distribution. Meanwhile, we indicate the possible measurement ranges for different materials, but these ranges are only reasonable references. In soft matter holographic measurements, the precise measurement range is related to the choice of recording wavelength and sample morphology. For an interferometric imaging system, the horizontal resolution depends on the selected magnification lens, while the axial resolution depends on the recording

Table 1   Cross-overview over the different materials and DH presented approaches

Soft matter	Method	Light Source	Measurement range	Sample feature
	WLI	White light	~50 nm to ~1.5 μm	Smooth liquid film with thickness less than 1.5 microns.
Thin-film	Off-axis DH	Visible laser	~300 nm to ~100 μm	Transparent film with continuous morphology.
	Hybrid approach	White light Visible laser	~50 nm to ~100 μm	All types of liquid film.
EHD drawn fiber Polymeric lens Micro-channel Hydrogels micro-scaffold Photoresist Surface Relief Grating	Off-axis DH	Visible laser	According to morphology and phase unwrapping.	Transparent or translucent soft- matter micro-structures with continuous thickness distribution and no-hollow structure.
Particles	In-line DH	Visible laser	Nanoscale particles moving in microscale.	Solution embedded particles.
	Off-axis DH	Visible laser	Microscale particles moving in milliscale.	Solution or films embedded particles.

wavelength and the minimum pixel size of the camera. Therefore, one of the advantages of holographic measurement is its adjustable measurement range and optimized measurement accuracy. Although holographic phase errors can be analyzed and calibrated through specific methods, the main measurement uncertainty still comes from the light source itself[133], which is different from interferometric measurement. The measurement error of interferometry arises from the number of observed interference fringes and the position of the sample[134–136]. This also implies that one of the reasons for choosing DH as the main measurement method for soft matter is that the placement of the sample does not affect the measurement accuracy.

The results reviewed here show that DH is robust in many challenging situations as it does not require frequent calibration while maintaining the attractive features of DH, that is, non-invasive, no-contrast agent, full-field imaging, high spatial resolution, and temporal high-frequency, up to the MHz range. We believe that DH has a bright future in the field of soft matter and advanced fabrication processes owing to its intrinsic capability to perform 3D imaging combined with quantitative analysis[137]. This idea is also supported by the increase in technological applications of thin films, from electronic to cosmic protective clothing and packaged water in gravity-free environments. Several other examples and published papers can be found discussing other challenging applications, we apologize if it was not possible to include all of them in this review.

Author details
¹CNR-ISASI, Institute of Applied Sciences and Intelligent Systems "E. Caianiello", Via Campi Flegrei 34, 80078 Pozzuoli, Napoli, Italy. ²Dipartimento di Ingegneria Chimica dei Materiali e della Produzione Industriale, Università degli Studi di Napoli "Federico II", Piazzale Tecchio 80, 80125 Napoli, Italy. ³NEAPoLIS, Numerical and Experimental Advanced Program on Liquids and Interface Systems, Joint Research Center CNR Università degli Studi di Napoli "Federico II", Napoli, Italy

Conflict of interest
The authors declare that they have no conflict of interest.

References
1. Stetson, K. A. & Powell, R. L. Interferometric hologram evaluation and real-time vibration analysis of diffuse objects. *Journal of the Optical Society of America* **55**, 1694-1695 (1965).
2. Rastogi, P. K. Holographic Interferometry: Principles and Methods. (Berlin: Springer, 2013).
3. Goodman, J. W. & Lawrence, R. W. Digital image formation from electronically detected holograms. *Applied Physics Letters* **11**, 77-79 (1967).
4. Schnars, U. & Jüptner, W. Direct recording of holograms by a CCD target and numerical reconstruction. *Applied Optics* **33**, 179-181 (1994).
5. Singh, V. R. & Asundi, A. In-line digital holography for dynamic metrology of MEMS. *Chinese Optics Letters* **7**, 1117-1122 (2009).

6. Lai, Y. W. et al. Integrity of micro-hotplates during high-temperature operation monitored by digital holographic microscopy. *Journal of Microelectromechanical Systems* **19**, 1175-1179 (2010).

7. Osten, W. Optical microsystems metrology. *Optics and Lasers in Engineering* **36**, 75-76 (2001).

8. Pedrini, G. et al. Calibration of optical systems for the measurement of microcomponents. *Optics and Lasers in Engineering* **47**, 203-210 (2009).

9. Matrecano, M. et al. Improving holographic reconstruction by automatic Butterworth filtering for microelectromechanical systems characterization. *Applied Optics* **54**, 3428-3432 (2015).

10. Pagliarulo, V. et al. Numerical tools for the characterization of microelectromechanical systems by digital holographic microscopy. *Journal of Micro/Nanolithography* **14**, 041314 (2015).

11. Grilli, S. et al. Whole optical wavefields reconstruction by digital holography. *Optics Express* **9**, 294-302 (2001).

12. Ferraro, P. et al. Compensation of the inherent wave front curvature in digital holographic coherent microscopy for quantitative phase-contrast imaging. *Applied Optics* **42**, 1938-1946 (2003).

13. Cuche, E., Bevilacqua, F. & Depeursinge, C. Digital holography for quantitative phase-contrast imaging. *Optics Letters* **24**, 291-293 (1999).

14. Kim, M. K. Principles and techniques of digital holographic microscopy. *SPIE Reviews* **1**, 018005 (2010).

15. Colomb, T. et al. Extended depth-of-focus by digital holographic microscopy. *Optics Letters* **35**, 1840-1842 (2010).

16. Fratz, M. et al. Digital holography in production: an overview. *Light:Advanced Manufacturing* **2**, 134-146 (2021).

17. Yang, L. et al. Multi-material multi-photon 3D laser micro-and nanoprinting. *Light:Advanced Manufacturing* **2**, 1-17 (2021).

18. Lee, A. et al. Optimization of experimental parameters to determine the jetting regimes in electrohydrodynamic printing. *Langmuir* **29**, 13630-13639 (2013).

19. Kim, M. K. Applications of digital holography in biomedical microscopy. *Journal of the Optical Society of Korea* **14**, 77-89 (2010).

20. Memmolo, P. et al. Breakthroughs in photonics 2013: holographic imaging. *IEEE Photonics Journal* **6**, 0701106 (2014).

21. Miccio, L. et al. Perspectives on liquid biopsy for label-free detection of "circulating tumor cells" through intelligent lab-on-chips. *View* **1**, 20200034 (2020).

22. Shaked, N. T. Quantitative phase microscopy of biological samples using a portable interferometer. *Optics Letters* **37**, 2016-2018 (2012).

23. Bishitz, Y. et al. Optical-mechanical signatures of cancer cells based on fluctuation profiles measured by interferometry. *Journal of Biophotonics* **7**, 624-630 (2014).

24. Park, Y. K., Depeursinge, C. & Popescu, G. Quantitative phase imaging in biomedicine. *Nature Photonics* **12**, 578-589 (2018).

25. Blum, O. & Shaked, N. T. Prediction of photothermal phase signatures from arbitrary plasmonic nanoparticles and experimental verification. *Light:Science & Applications* **4**, e322 (2015).

26. Kuschmierz, R. et al. Ultra-thin 3D lensless fiber endoscopy using diffractive optical elements and deep neural networks. *Light:Advanced Manufacturing* **2**, 1-10 (2021).

27. Mysels, K. J. Soap films and some problems in surface and colloid chemistry. *The Journal of Physical Chemistry* **68**, 3441-3448 (1964).

28. Hartl, M. et al. Thin film colorimetric interferometry. *Tribology Transactions* **44**, 270-276 (2001).

29. Israelachvili, J. N. Thin film studies using multiple-beam interferometry. *Journal of Colloid and Interface Science* **44**, 259-272 (1973).

30. Kim, S. W. & Kim, G. H. Thickness-profile measurement of transparent thin-film layers by white-light scanning interferometry. *Applied Optics*

31. Chen, H. et al. Structural coloration by internal reflection and interference in hydrogel microbubbles and their precursors. *Advanced Optical Materials* **9**, 2100259 (2021).

32. Afanasyev, Y. D., Andrews, G. T. & Deacon, C. G. Measuring soap bubble thickness with color matching. *American Journal of Physics* **79**, 1079-1082 (2011).

33. Kitagawa, K. Thin-film thickness profile measurement by three-wavelength interference color analysis. *Applied Optics* **52**, 1998-2007 (2013).

34. Vannoni, M. et al. Measuring the thickness of soap bubbles with phase-shift interferometry. *Optics Express* **21**, 19657-19667 (2013).

35. Gao, F., Muhamedsalih, H. & Jiang, X. Q. Surface and thickness measurement of a transparent film using wavelength scanning interferometry. *Optics Express* **20**, 21450-21456 (2012).

36. Mandracchia, B. et al. Quantitative imaging of the complexity in liquid bubbles' evolution reveals the dynamics of film retraction. *Light:Science & Applications* **8**, 20 (2019).

37. Wong, W. S. Y. et al. Super liquid repellent surfaces for anti-foaming and froth management. *Nature Communications* **12**, 5358 (2021).

38. Osten, W. Optical Inspection of Microsystems. (Boca Raton: CRC Press, 2018).

39. Ferraro, P. et al. Extended focused image in microscopy by digital holography. *Optics Express* **13**, 6738-6749 (2005).

40. Zhang, J. et al. A review of common-path off-axis digital holography: towards high stable optical instrument manufacturing. *Light:Advanced Manufacturing* **2**, 1-17 (2021).

41. Wang, Z. et al. Interferometric measurement of film thickness during bubble blowing. Proceedings of SPIE 10333, Optical Methods for Inspection, Characterization, and Imaging of Biomaterials III. Munich, Germany: SPIE, 2017.

42. Joye, J. L., Hirasaki. G. J. & Miller, C. A. Dimple formation and behavior during axisymmetrical foam film drainage. *Langmuir* **8**, 3083-3092 (1992).

43. Bioucas-Dias, J. M. & Valadao, G. Phase unwrapping via graph cuts. *IEEE Transactions on Image Processing* **16**, 698-709 (2007).

44. Sett, S., Sinha-Ray, S. & Yarin, A. L. Gravitational drainage of foam films. *Langmuir* **29**, 4934-4947 (2013).

45. Schnars, U. et al. Digital holography. in Digital Holography and Wavefront Sensing: Principles, Techniques and Applications (eds Schnars, U. et al.) (Berlin, Heidelberg: Springer, 2014), 39-68.

46. Huang, T. S. Digital holography. *Proceedings of the IEEE* **59**, 1335-1346 (1971).

47. González-Cano, A. & Bernabéu, E. Automatic interference method for measuring transparent film thickness. *Applied Optics* **32**, 2292-2294 (1993).

48. Ferraro, V. et al. Full-field and quantitative analysis of a thin liquid film at the nanoscale by combining digital holography and white light interferometry. *The Journal of Physical Chemistry C* **125**, 1075-1086 (2021).

49. Hoyt, L. F. & Verwiebe, A. Determination of the concentration of liquid soaps by the immersion refractometer. *Industrial & Engineering Chemistry* **18**, 581-582 (1926).

50. Glassner, A. Soap bubbles : part 2. *IEEE Computer Graphics and Applications* **2**, 99-109 (2000).

51. Osten, W. et al. Recent advances in digital holography. *Applied Optics* **53**, G44-G63 (2014).

52. Ferraro, V. et al. Axisymmetric bare freestanding films of highly viscous liquids: preparation and real-time investigation of capillary leveling. *Journal of Colloid and Interface Science* **596**, 493-499 (2021).

53. Kim, Y. et al. Surface measurement of indium tin oxide thin film by wavelength-tuning Fizeau interferometry. *Applied Optics* **54**, 7135-

38, 5968-5973 (1999).

7141 (2015).

54. Zhang, Y. R. et al. Nanoscopic terraces, mesas, and ridges in freely standing thin films sculpted by supramolecular oscillatory surface forces. *ACS Nano* **10**, 4678-4683 (2016).

55. Piegari, A. & Masetti, E. Thin film thickness measurement: a comparison of various techniques. *Thin Solid Films* **124**, 249-257 (1985).

56. Onses, M. S. et al. Mechanisms, capabilities, and applications of high-resolution electrohydrodynamic jet printing. *Small* **11**, 4237-4266 (2015).

57. Ferraro, P. et al. Dispensing nano–pico droplets and liquid patterning by pyroelectrodynamic shooting. *Nature Nanotechnology* **5**, 429-435 (2010).

58. Coppola, S. et al. Self-assembling of multi-jets by pyro-electrohydrodynamic effect for high throughput liquid nanodrops transfer. *Lab on a Chip* **11**, 3294-3298 (2011).

59. Gennari, O. et al. Investigation on cone jetting regimes of liquid droplets subjected to pyroelectric fields induced by laser blasts. *Applied Physics Letters* **106**, 054103 (2015).

60. Coppola, S. et al. Nanocomposite polymer carbon-black coating for triggering pyro-electrohydrodynamic inkjet printing. *Applied Physics Letters* **106**, 261603 (2015).

61. Ruggiero, F. et al. Electro-drawn polymer microneedle arrays with controlled shape and dimension. *Sensors and Actuators B:Chemical* **255**, 1553-1560 (2018).

62. Coppola, S. et al. On the spraying modality of liquids by pyroelectrohydrodynamics. *ACS Omega* **3**, 17707-17716 (2018).

63. Madugani, R. et al. Terahertz tuning of whispering gallery modes in a PDMS stand-alone, stretchable microsphere. *Optics Letters* **37**, 4762-4764 (2012).

64. Russo, P. et al. Single fibres of pyro-electrospinned PVDF-HFP/MWCNT unveal high electrical conductivity. *Polymer* **159**, 157-161 (2018).

65. Hayati, I., Bailey, A. & Tadros, T. F. Investigations into the mechanism of electrohydrodynamic spraying of liquids: II. Mechanism of stable jet formation and electrical forces acting on a liquid cone. *Journal of Colloid and Interface Science* **117**, 222-230 (1987).

66. Jaworek, A. & Krupa, A. Jet and drops formation in electrohydrodynamic spraying of liquids. A systematic approach. *Experiments in Fluids* **27**, 43-52 (1999).

67. Jaworek, A. & Krupa, A. Generation and characteristics of the precession mode of EHD spraying. *Journal of Aerosol Science* **27**, 75-82 (1996).

68. Gim, Y. et al. Development of limited-view and three-dimensional reconstruction method for analysis of electrohydrodynamic jetting behavior. *Optics Express* **25**, 9244-9251 (2017).

69. Atkinson, C. & Soria, J. An efficient simultaneous reconstruction technique for tomographic particle image velocimetry. *Experiments in Fluids* **47**, 553-568 (2009).

70. Lu, W. K. & Yin, F. F. Adaptive algebraic reconstruction technique: adaptive algebraic reconstruction technique. *Medical Physics* **31**, 3222-3230 (2004).

71. Verhoeven, D. Limited-data computed tomography algorithms for the physical sciences. *Applied Optics* **32**, 3736-3754 (1993).

72. Edwards, C. et al. Measuring the nonuniform evaporation dynamics of sprayed sessile microdroplets with quantitative phase imaging. *Langmuir* **31**, 11020-11032 (2015).

73. Polonschii, C. et al. High-resolution impedance mapping using electrically activated quantitative phase imaging. *Light:Science & Applications* **10**, 20 (2021).

74. Yokota, M. & Aoyama, F. Drying process of an ink-dot analyzed using both digital holographic microscopy and tackiness measurement.

Microelectronic Engineering **241**, 111543 (2021).

75. Yao, L. C. et al. Three-dimensional dynamic measurement of irregular stringy objects via digital holography. *Optics Letters* **43**, 1283-1286 (2018).

76. Lebrun, D. et al. Particle field digital holographic reconstruction in arbitrary tilted planes. *Optics Express* **11**, 224-229 (2003).

77. Kempkes, M. et al. Three dimensional digital holographic profiling of micro-fibers. *Optics Express* **17**, 2938-2943 (2009).

78. Wu, Y. C. et al. Wavelet-based depth-of-field extension, accurate autofocusing, and particle pairing for digital inline particle holography. *Applied Optics* **53**, 556-564 (2014).

79. Busse, F. et al. Digital interference microscopy and density reconstruction of picosecond infrared laser desorption at the water-air interface. *Journal of Applied Physics* **124**, 094701 (2018).

80. Guildenbecher, D R. et al. Digital holography simulations and experiments to quantify the accuracy of 3D particle location and 2D sizing using a proposed hybrid method. *Applied Optics* **52**, 3790-3801 (2013).

81. Coppola, S. et al. Tethered pyro-electrohydrodynamic spinning for patterning well-ordered structures at micro-and nanoscale. *Chemistry of Materials* **26**, 3357-3360 (2014).

82. Coppola, S. et al. Layered 3D printing by tethered pyro-electrospinning. *Advances in Polymer Technology* **2020**, 1252960 (2020).

83. Grilli, S. et al. 3D lithography by rapid curing of the liquid instabilities at nanoscale. *Proceedings of the National Academy of Sciences of the United States of America* **108**, 15106-15111 (2011).

84. Mecozzi, L. et al. Easy printing of high viscous microdots by spontaneous breakup of thin fibers. *ACS applied materials & interfaces* **10**, 2122-2129 (2018).

85. Vespini, V. et al. Forward electrohydrodynamic inkjet printing of optical microlenses on microfluidic devices. *Lab on a Chip* **16**, 326-333 (2016).

86. Bianco, V. et al. Endowing a plain fluidic chip with micro-optics: a holographic microscope slide. *Light:Science & Applications* **6**, e17055 (2017).

87. Camou, S., Fujita, H. & Fujii, T. PDMS 2D optical lens integrated with microfluidic channels: principle and characterization. *Lab on a Chip* **3**, 40-45 (2003).

88. Liu, S. H. et al. Assembly and alignment of metallic nanorods on surfaces with patterned wettability. *Small* **2**, 1448-1453 (2006).

89. Mugele, F. & Herminghaus, S. Electrostatic stabilization of fluid microstructures. *Applied Physics Letters* **81**, 2303-2305 (2002).

90. Psaltis, D., Quake, S. R. & Yang, C. Developing optofluidic technology through the fusion of microfluidics and optics. *Nature* **442**, 381-386 (2006).

91. Jones, T. B. et al. Dielectrophoretic liquid actuation and nanodroplet formation. *Journal of Applied Physics* **89**, 1441-1448 (2001).

92. Mugele, F. & Baret, J. C. Electrowetting: from basics to applications. *Journal of Physics:Condensed Matter* **17**, R705-R774 (2005).

93. Wang, D. B. et al. Local wettability modification by thermochemical nanolithography with write-read-overwrite capability. *Applied Physics Letters* **91**, 243104 (2007).

94. Hayes, R A. & Feenstra, B. J. Video-speed electronic paper based on electrowetting. *Nature* **425**, 383-385 (2003).

95. Moran, P. M. et al. Fluidic lenses with variable focal length. *Applied Physics Letters* **88**, 041120 (2006).

96. Bourim, E. M. et al. Investigation of pyroelectric electron emission from monodomain lithium niobate single crystals. *Physica B:Condensed Matter* **383**, 171-182 (2006).

97. Ferraro, P. et al. Wettability patterning of lithium niobate substrate by modulating pyroelectric effect to form microarray of sessile droplets.

Applied Physics Letters **92**, 213107 (2008).

98. Grilli, S. et al. Liquid micro-lens array activated by selective electrowetting on lithium niobate substrates. *Optics Express* **16**, 8084-8093 (2008).

99. Miccio, L. et al. Tunable liquid microlens arrays in electrode-less configuration and their accurate characterization by interference microscopy. *Optics Express* **17**, 2487-2499 (2009).

100. Miccio, L. et al. Hemicylindrical and toroidal liquid microlens formed by pyro-electro-wetting. *Optics Letters* **34**, 1075-1077 (2009).

101. Grimaldi, I. A. et al. Graded-size microlens array by the pyro-electrohydrodynamic continuous printing method. *Applied Optics* **52**, 7699-7705 (2013).

102. Coppola, S. et al. Direct writing of microfluidic footpaths by pyro-EHD printing. *ACS Applied Materials & Interfaces* **9**, 16488-16494 (2017).

103. Ricotti, L. et al. Quantification of growth and differentiation of C2C12 skeletal muscle cells on PSS–PAH-based polyelectrolyte layer-by-layer nanofilms. *Biomedical Materials* **6**, 031001 (2011).

104. Aubin, H. et al. Directed 3D cell alignment and elongation in microengineered hydrogels. *Biomaterials* **31**, 6941-6951 (2010).

105. Ahadian, S. et al. Moldable elastomeric polyester-carbon nanotube scaffolds for cardiac tissue engineering. *Acta Biomaterialia* **52**, 81-91 (2017).

106. Kim, S. et al. Fabrication and characterization of magnetic microrobots for three-dimensional cell culture and targeted transportation. *Advanced Materials* **25**, 5863-5868 (2013).

107. Li, X. *et al*. Holographic display-based control for high-accuracy photolithography of cellular micro-scaffold with heterogeneous architecture. *IEEE/ASME Transactions on Mechatronics*. http://dx.doi.org/10.1109/TMECH.2021.3081769 (2021).

108. Toulouse, A. et al. 3D-printed miniature spectrometer for the visible range with a 100×100 μm^2 footprint. *Light:Advanced Manufacturing* **2**, 2 (2021).

109. Saha, S. K. et al. Scalable submicrometer additive manufacturing. *Science* **366**, 105-109 (2019).

110. Besaga, V. R. et al. Monitoring of photochemically induced changes in phase-modulating samples with digital holographic microscopy. *Applied Optics* **58**, G41-G47 (2019).

111. Zhao, X. & Rosen, D. W. Real-time interferometric monitoring and measuring of photopolymerization based stereolithographic additive manufacturing process: sensor model and algorithm. *Measurement Science and Technology* **28**, 015001 (2016).

112. Pagliarulo, V. et al. Direct quantitative imaging of the writing stage in a photosensitive azopolymer by digital holography. *Soft Matter* **15**, 7809-7813 (2019).

113. Rekola, H. et al. Digital holographic microscopy for real-time observation of surface-relief grating formation on azobenzene-containing films. *Scientific Reports* **10**, 19642 (2020).

114. Jith, A., Kumar, P. T. A. & Kumaran, R. K. Digital holographic method to study stress formation in photopolymer during live recording of holograms. *Optical Engineering* **60**, 035105 (2021).

115. Chikode, P. P. et al. Deformation studies of cylindrical nanostructured silica aerogels by using phase shifting digital holographic interferometry. *Materials Today:Proceedings* **46**, 2298-2306 (2021).

116. Yu, X. et al. Measurement of Young's modulus of polyacrylamide gel by digital holography. Digital Holography and Three-Dimensional Imaging 2011. Tokyo Japan: Optical Society of America, 2011.

117. Wang, C. et al. Celebrating *Soft Matter's* 10th Anniversary: monitoring colloidal growth with holographic microscopy. *Soft Matter* **11**, 1062-1066 (2015).

118. Fung, J. et al. Imaging multiple colloidal particles by fitting electromagnetic scattering solutions to digital holograms. *Journal of Quantitative Spectroscopy and Radiative Transfer* **113**, 2482-2489 (2012).

119. Krishnatreya, B. J. et al. Measuring Boltzmann's constant through holographic video microscopy of a single colloidal sphere. *American Journal of Physics* **82**, 23-31 (2014).

120. Cheong, F. C. et al. Holographic characterization of colloidal particles in turbid media. *Applied Physics Letters* **111**, 153702 (2017).

121. Middleton, C. et al. Optimizing the synthesis of monodisperse colloidal spheres using holographic particle characterization. *Langmuir* **35**, 6602-6609 (2019).

122. Gupta, S. & Vanapalli, S. A. Microfluidic shear rheology and wall-slip of viscoelastic fluids using holography-based flow kinematics. *Physics of Fluids* **32**, 012006 (2020).

123. Koukourakis, N. et al. Wavefront shaping for imaging-based flow velocity measurements through distortions using a Fresnel guide star. *Optics Express* **24**, 22074-22087 (2016).

124. Panahi, M. et al. 3D monitoring of the surface slippage effect on micro-particle sedimentation by digital holographic microscopy. *Scientific Reports* **11**, 12916 (2021).

125. Wu, Y. C. et al. Quantifying bubble size and 3D velocity in a vortex with digital holographic particle tracking velocimetry (DHPTV). *Flow Measurement and Instrumentation* **76**, 101826 (2020).

126. Meng, H. et al. Holographic particle image velocimetry: from film to digital recording. *Measurement Science and Technology* **15**, 673-685 (2004).

127. Gao, Z. Y. et al. Distortion correction for particle image velocimetry using multiple-input deep convolutional neural network and Hartmann-Shack sensing. *Optics Express* **29**, 18669-18687 (2021).

128. Altman, L. E. & Grier, D. G. CATCH: characterizing and tracking colloids holographically using deep neural networks. *The Journal of Physical Chemistry B* **124**, 1602-1610 (2020).

129. Midtvedt, D. Deep learning enhanced digital holography for characterization of nanoparticles and soft matter. Proceedings of SPIE 11804, Emerging Topics in Artificial Intelligence (ETAI) 2021. San Diego, California, United States: SPIE, 2021.

130. Midtvedt, B. et al. Fast and accurate nanoparticle characterization using deep-learning-enhanced off-axis holography. *ACS Nano* **15**, 2240-2250 (2021).

131. Lu, S. Y. et al. Dynamic quantitative phase imaging based on Ynet-ConvLSTM neural network. *Optics and Lasers in Engineering* **150**, 106833 (2022).

132. Forouhesh Tehrani, K. et al. In situ measurement of the isoplanatic patch for imaging through intact bone. *Journal of Biophotonics* **14**, e202000160 (2021).

133. Thurman, S. T. & Fienup, J. R. Phase-error correction in digital holography. *Journal of the Optical Society of America A* **25**, 983-994 (2008).

134. Lowman, A. E. & Greivenkamp, J. E. Interferometer errors due to the presence of fringes. *Applied Optics* **35**, 6826-6828 (1996).

135. Berger, R., Sure, T. & Osten, W. Measurement errors of mirrorlike, tilted objects in white light interferometry. Proceedings of SPIE 6616, Optical Measurement Systems for Industrial Inspection V. Munich, Germany: SPIE, 2007.

136. Pruss, C. et al. Computer-generated holograms in interferometric testing. *Optical Engineering* **43**, 2534-2540 (2004).

137. Sheridan, J. T. et al. Roadmap on holography. *Journal of Optics* **22**, 123002 (2020).